VIBRATIONAL ENERGY TRANSFER IN ORTHO AND PARA NH_3

VIBRATIONAL ENERGY TRANSFER IN ORTHO AND PARA NH_3

By

DAVID JOHN DANAGHER, B. Sc.

A Thesis

Submitted to the School of Graduate Studies

in Partial Fulfilment of the Requirements

for the Degree

Master of Science

McMaster University

September 1986

MASTER OF SCIENCE (1986) McMASTER UNIVERSITY

(Physics)

TITLE: VIBRATIONAL ENERGY TRANSFER IN ORTHO AND PARA NH_3

AUTHOR: David J. Danagher, B. Sc. University of Waterloo

SUPERVISOR: Dr. John Reid

NUMBER OF PAGES: 61

ABSTRACT

An experimental study of vibrational energy transfer in ortho and para $NH_3(\nu_2)$ is presented. The vibrational relaxation rates are necessary to characterize mid-IR pulsed and cw NH_3 lasers, and the interpretation of these rates is of theoretical importance. Accurate information on the (V-T) process in NH_3/N_2 mixtures and the (V-V) energy transfer between ortho and para $^{15}NH_3$ and $^{14}NH_3$ is now available.

First, NH_3 linestrengths and linewidths were accurately measured with a tunable diode laser (TDL) so that ammonia concentrations could be calculated from TDL scans. The energy transfer mechanisms were studied by exciting the ν_2 vibration of NH_3 with a Q-switched CO_2 laser and probing the subsequent changes in population with a TDL. A difference in ν_2 lifetimes was observed between ortho and para NH_3 transitions, and is explained by a (V-V) transfer of energy between the NH_3 species. An isolated ortho $^{15}NH_3$ absorption line was pumped and vibrational transfer of energy was observed to ortho and para $^{14}NH_3$ and $^{15}NH_3$.

ACKNOWLEDGEMENTS

I sincerely thank my supervisor, Dr. John Reid for his guidance and support in this research.

I also wish to thank Ed Williams, Dr. T. Oka, Pierre Cherrier, Paul Beckwith, and the McMaster/ Hamilton community for their many contributions to this work.

Finally, I especially thank my family for helping me through my education.

TABLE OF CONTENTS

LIST OF FIGURES

LIST OF TABLES

CHAPTER 1

INTRODUCTION

Collisional relaxation processes in gases have long been of interest to both experimentalists and theorists alike. For example, the dynamics of all gas lasers are very strongly influenced by the relaxation mechanisms of the active molecules or atoms, while theorists use measured relaxation rates to determine the nature of collisional processes in gases. The case of vibrational to translational (V-T) energy transfer of the ν_2 vibration of NH_3 has both practical and theoretical interest. This rate plays a major role in the dynamics of pulsed and cw 12-μm NH_3 lasers developed in the early 1980's.[1-4] In particular, the successful modelling of the recently developed line tunable cw NH_3 laser requires an accurate knowledge of the ν_2 mode relaxation rate.[3] The (V-T) rate is known to be very rapid in NH_3 as is the case in other hydrogen bonded systems, and the interpretation of these rates is of theoretical importance.[5] Recent measurements of (V-T) transfer rates for NH_3 are summarized in two papers by Hovis and Moore.[5,6] Hovis and Moore used a pulsed CO_2 laser to excite the $NH_3(\nu_2)$ level and observe fluorescence from the entire ν_2 band to make detailed measurements of the (V-T) rate in mixtures of NH_3 with several buffer gases. In these

experiments Hovis and Moore were unable to separately study the relaxation rates of the individual vibrational-rotational levels in NH_3, and concluded that "experimental and theoretical studies of rates with resolved initial and final rotational states could give a better understanding of the role that rotation plays."

In view of these comments, and the importance of the v_2 level in NH_3 lasers, a new apparatus was designed to measure relaxation rates in NH_3 gas mixtures. The apparatus consists of a tunable lead salt diode laser which probes changes in absorption induced in a gas by a pulse from a Q-switched CO_2 laser. In this study, results were obtained by studying mixtures of $^{14}NH_3$ and $^{15}NH_3$ in N_2 at temperatures of 200 and 300 K. While the average (V-T) relaxation rates are in satisfactory agreement with the results of Hovis and Moore, the improved accuracy of the TDL (tunable diode laser) measurements coupled with the ability to investigate relaxation rates for individual vibrational-rotational levels has resulted in the measurement of V-V transfer rates between ortho and para NH_3. The existence of this slow transfer mechanism was deduced from infrared-microwave double resonance studies by Kano et al.[7,8] In the present study, V-V transfer results in different lifetimes for vibrationally excited ortho and para NH_3.

The purpose of this study is to experimentally determine (V-T) and (V-V) transfer rates in NH_3 gas mixtures.

Chapter 2 describes the molecular structure of NH_3 and possible (V-T) and (V-V) vibrational energy transfer mechanisms. The method of determining the NH_3 concentration in mixtures using a TDL is described in Chapter 3, along with initial measurements of ν_2 lifetimes. In Chapter 4, the (V-T) rates associated with NH_3-NH_3 and NH_3-N_2 collisions are determined, and a (V-V) energy transfer mechanism between the NH_3 ortho and para species is shown to be responsible for different ν_2 lifetimes. Vibrational energy transfer between $^{14}NH_3$ and $^{15}NH_3$ is also observed. Finally, in Chapter 5 the sensitivity of this transient detection system is examined and future studies in transient detection are suggested, including the possibility of a fast, sensitive NH_3 detector.

CHAPTER 2

VIBRATIONAL ENERGY IN NH_3

2.1 Introduction

This chapter summarizes the vibrational energy levels in NH_3 and their relation to pulsed and cw mid-infrared NH_3 lasers. The molecular structure of NH_3 will be examined and the mechanisms of energy transfer between vibrational-rotational energy levels will be discussed. These energy transfer processes are important in understanding the dynamics of mid-IR NH_3 lasers. A rate equation model of NH_3 lasers developed by Morrison[9] will be outlined.

2.2 Molecular structure of NH_3

The NH_3 molecule has three-fold rotational symmetry[10] with four normal modes of vibration. Optically pumped pulsed mid-IR lasers have operated between the (ν_2-ground) and ($2\nu_2$-ν_2) vibrational levels of both $^{14}NH_3$ and $^{15}NH_3$, and cw lasing has been observed on (ν_2-ground) state transitions. The NH_3 energy levels relevant to mid-IR lasers are shown in Figure 2.1. The three hydrogen nuclei in NH_3 act as a potential barrier through which the nitrogen nucleus can tunnel. As a result the ν_2 levels are split into levels labelled symmetric (s) and antisymmetric (a). Energy stored in rotational motion is labelled by quantum numbers J and K

FIGURE 2.1 $NH_3(\nu_2)$ energy spectrum. Mid-IR laser action has been observed on (ν_2-ground) transitions and a$\rightarrow$s ($2\nu_2 - \nu_2$) transitions which span the 11-13 μm and 16-21 μm wavelength regions respectively.

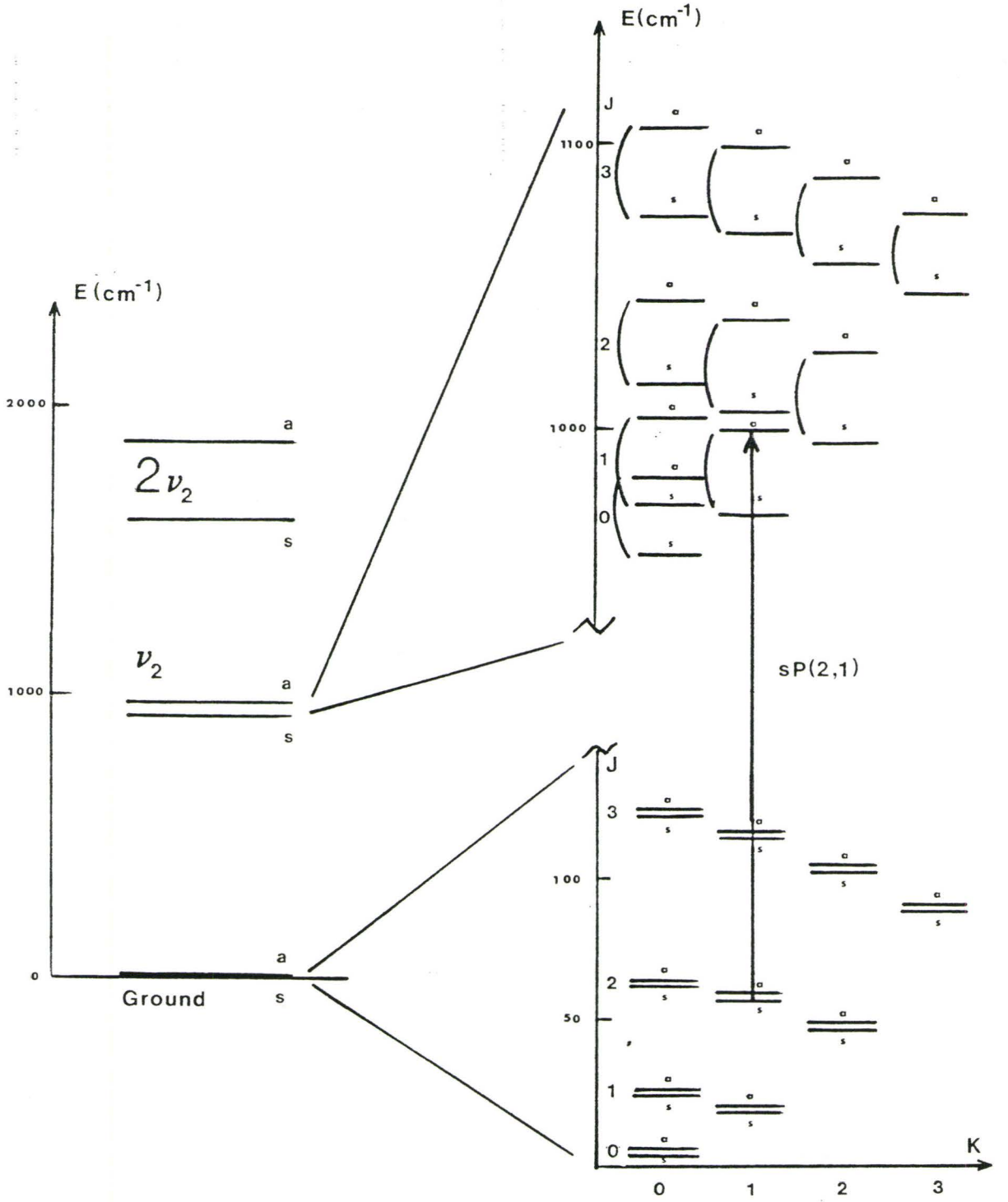
E(cm-1)
2000
1000
0
a
2ν2
s
ν2
a
s
a
Ground
s
E(cm-1)
J
1100
3
2
1000
1
0
sP(2,1)
J
3
100
2
50
1
0
K
0
1
2
3

and the rotational energy is approximately $BJ(J+1)+(C-B)K^2$. The molecular constants B and C are inversely proportional to the moments of inertia.[11] Electric dipole transitions must obey the following selection rules:[10]

(a) a $\leftrightarrow$ s

(b) $\Delta J = -1, 0, 1$ if $K \neq 0$

$\Delta J = \pm 1$ if $K = 0$

(c) $\Delta K = 0$ => ortho $\leftrightarrow$ ortho $(K=3n)$

para $\leftrightarrow$ para $(K=3n\pm1)$

Thus (ν_2-ground) transitions are labelled xY(J,K) where x = a or s, and Y = P, Q, or R corresponding to changes in J of -1, 0, or 1. Similarly ($2\nu_2-\nu_2$) transitions are labelled 2xY(J,K). The final rule (c) forbids radiative transfer between ortho levels (K=3n) and para levels ($K=3n\pm1$)

2.3 Vibrational Energy Transfer and NH_3 Lasers

When a molecular gas is confined in a thermally insulated container, the system will eventually reach an equilibrium condition in which the net energy flow into or out of any particular vibrational-rotational level is zero. Vibrational energy is continually exchanged within the thermal equilibrium through spontaneous emission of radiation or collisions. In a molecular gas such as NH_3, the spontaneous emission lifetimes of vibrational levels is typically 0.01 s - 1.0 s,[12] which is generally much longer than energy transferred via collisions. The energy transfer

mechanisms studied in this thesis result from two collisional processes, vibration to translation (V-T) energy transfer, and vibration to vibration (V-V) energy transfer. Both processes occur much faster than the spontaneous emission lifetimes and the latter effect does not significantly contribute to the rate at which the NH_3 vibrational levels reach equilibrium.

Classically, (V-T) energy transfer can be represented by two vibrating masses connected by a spring colliding with a third mass. During the collision, energy stored in the vibration of the diatomic "molecule" may be transferred to or from the translational energy of the system. To model energy transfer during a collision of molecules in a gas, the effect of a suitable interaction potential can be calculated using the Born approximation. The results of such calculations[12] indicate that usually only one quantum of vibrational energy is converted into translational or rotational energy such as

$$NH_3(v_2=1) + N_2 \rightarrow NH_3(v_2=0) + N_2 + \Delta E$$

The energy difference between the levels is converted into kinetic energy of the NH_3 and N_2 molecules. In a (V-V) process, energy flows from one vibrational state to another with relatively little conversion to translational energy. A typical (V-V) process is described as follows:

$$CO(1) + NO(0) \rightarrow CO(0) + NO(1) + \Delta E$$

In this process, energy is transferred from one molecule to another, and the leftover energy is converted to

translational or rotational energy of the molecule. Similarly energy can be transferred from one vibrational mode to another within the same molecule:

$$CO_2(00^01) + N_2 \rightarrow CO_2(10^00) + N_2 + \Delta E$$

Many (V-V) processes are possible but usually the dominant (fastest) mechanisms are those that are near resonance and require the fewest number of quantum number changes.

Experimentally, (V-V) and (V-T) processes can be studied by upsetting the conditions of thermal equilibrium and observing the time response of the system to return to equilibrium. In polyatomic systems there are many levels so that the possible vibrational exchanges are numerous. A pulsed laser/ probe laser system is advantageous since a particular transition can be excited and any other level may be probed making it possible to separately study the many (V-V) and (V-T) processes taking place. In NH_3, the relevant paths of energy transfer are shown in Figure 2.2.

In previous work Hovis and Moore[5,6] measured τ_{VT} by exciting the ν_2 level with a CO_2 pulsed laser and observing the fluorescence signal from the entire ν_2 band. Individual rotational levels could not be probed. The rates that were measured in the present work are τ_{VT} for individual rotational levels for NH_3-NH_3 and NH_3-N_2 collisions, and τ_{VV} rate between ortho and para $^{14}NH_3$ and $^{15}NH_3$. By probing individual rotational transitions, the dependence of vibrational energy transfer on J, K, symmetry and species has

FIGURE 2.2 Paths of vibrational-rotational energy transfer in NH_3. The rates measured in this work are τ_{VT} for NH_3-NH_3 and NH_3-N_2 collisions, and τ_{VV} between ortho and para species of $^{14}NH_3$ and $^{15}NH_3$.

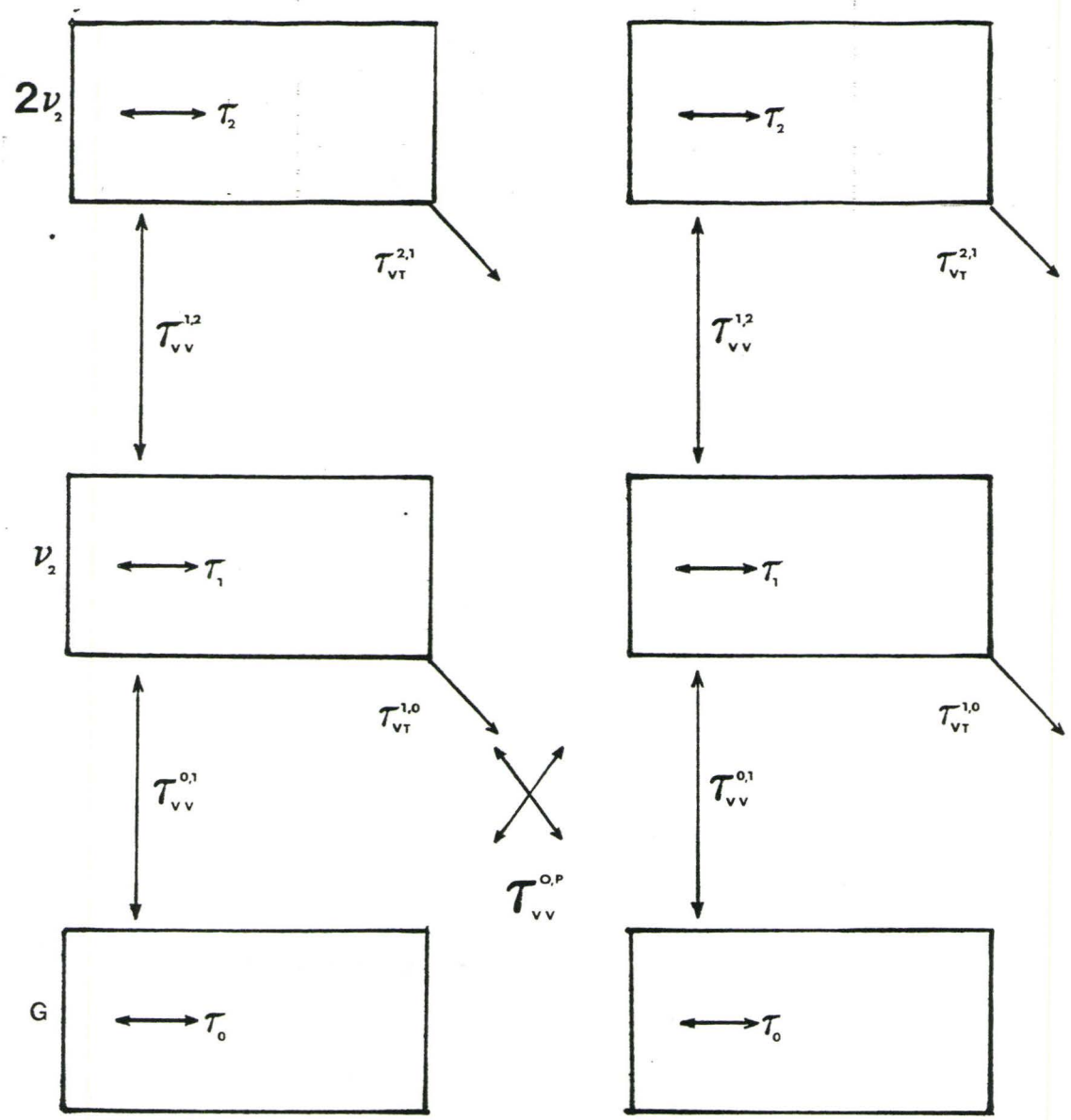

ORTHO NH_3 PARA NH_3

been determined.

In mid-IR NH_3 lasers, a CO_2 laser in resonance with a single R branch (ν_2-ground) transition transfers population to the entire ν_2 level through very fast rotational relaxation.[1-3] Population inversion and gain are observed on many 11-13 μm transitions and this laser system has been accurately modelled by a rate equation model.[3] A thermalized rotational distribution in the ν_2=0 and 1 levels is assumed since the rotational relaxation rate is very fast compared to (V-T) or (V-V) rates. The ortho and para species are treated completely separate in the model since Kroeker,[13,14] Sinclair,[3] and Morrison[9] have observed that laser action can only be obtained in the ortho species if an ortho transition is excited, and to obtain laser action on the para species, a para transition must be pumped. The basis of the model is a set of four rate equations which describe the time evolution of the ground, ν_2, and $2\nu_2$ vibrational levels, as well as the two directly pumped rotational levels. Contained in these equations are the rotational relaxation rates τ_0 and τ_1, the (V-T) rate τ_{VT}, and the (V-V) transfer rate to higher levels τ_{VV}. Hence an accurate knowledge of these rates is necessary to model the mid-IR NH_3 laser. The experimental results reported in this thesis provide many of the required relaxation rates for the rate equation model of NH_3 laser dynamics.

2.4 Summary

The above discussion has summarized the spectroscopy and vibrational energy transfer mechanisms relevant to the ν_2 level of NH_3. The rates can be studied by perturbing the thermal equlibrium of the system with a pulsed laser and observing the time evolution of the populations with a cw probe laser. The following chapters describe how the (V-T) rate and (V-V) transfer rates between ortho and para species of $^{14}NH_3$ and $^{15}NH_3$ were measured with a tunable diode laser.

CHAPTER 3

EXPERIMENTAL DETERMINATION OF $NH_3(\nu_2)$ LIFETIMES

3.1 Introduction

The (V-T) and (V-V) energy transfer mechanisms in the ν_2 level has practical interest because of the direct link to NH_3 mid-infrared lasers as shown in Chapter 2. The (V-T) rate is rapid in NH_3 and other hydrogen bonded systems and these rates are also of theoretical importance. In this chapter the measurement of the $NH_3(\nu_2)$ lifetime with a tunable diode laser will be discussed. The following section describes how NH_3 linestrengths and NH_3 in N_2 linewidths were measured accurately so the NH_3 concentration could be calculated from TDL scans of the ν_2 absorption lines. Section 3.3 describes the experimental apparatus used to observe transient population changes in $NH_3(\nu_2)$. The final section explains how the transient absorption can be related to the ν_2 lifetimes, and gives the initial results of the experiment.

3.2 Determination of NH_3 Concentration

Using a chopper, lock-in amplifier, and conventional amplitude detection, high resolution scans of NH_3 absorption vs. frequency are routinely recorded using a TDL. To determine an accurate NH_3 concentration from scans of NH_3 in

N_2 mixtures, accurate values of the linestrengths, S, and pressure broadened linewidths, γ, are required. Pressure broadening coefficients for NH_3 in N_2 mixtures were not available in the literature so a series of measurements of S and γ were made in conventional gas cells.

The output characteristics (wavelength vs. current, temperature) of the TDL were determined using a monochromator. A lock-in amplifier was used to process the chopped signal, and an Ithaco 385E0-2 analog-to-digital converter interfaced the lock-in amplifier to the PC. A cell length ranging from 0.57 cm to 15.0 cm was chosen so that linecenter absorptions ranged from 20 - 60 % in a single pass. To ensure that the diode was operating in single mode (i.e., at only one wavelength), a cell with several Torr of pure NH_3 was placed in the beam and the zero transmission baseline was monitored. The TDL was tuned with a Ge etalon (fringe spacing = 0.01627 cm^{-1}) in the beam and the tuning rate was measured. The absorption coefficient was calculated as a function of wavelength and a Voigt profile[15] was fitted to the data. The deviation in the fit is at worst 1 % as shown in Figure 3.1. Absorption scans were taken at several pressures and the Voigt profile fits were used to determine the linewidth. Results with low NH_3 concentration mixtures (see Table 3.1) showed that N_2 and Ar pressure broadening coefficients vary from transition to transition. NH_3 linestrengths and pressure broadening coefficients were

FIGURE 3.1 Measured and calculated lineshapes of an NH_3 absorption line in a 0.57 cm cell. The residuals (upper scan) are shown as a percentage of the line center absorption. Similar scans were recorded on other NH_3 lines to obtain accurate linestrengths and pressure broadened linewidths.

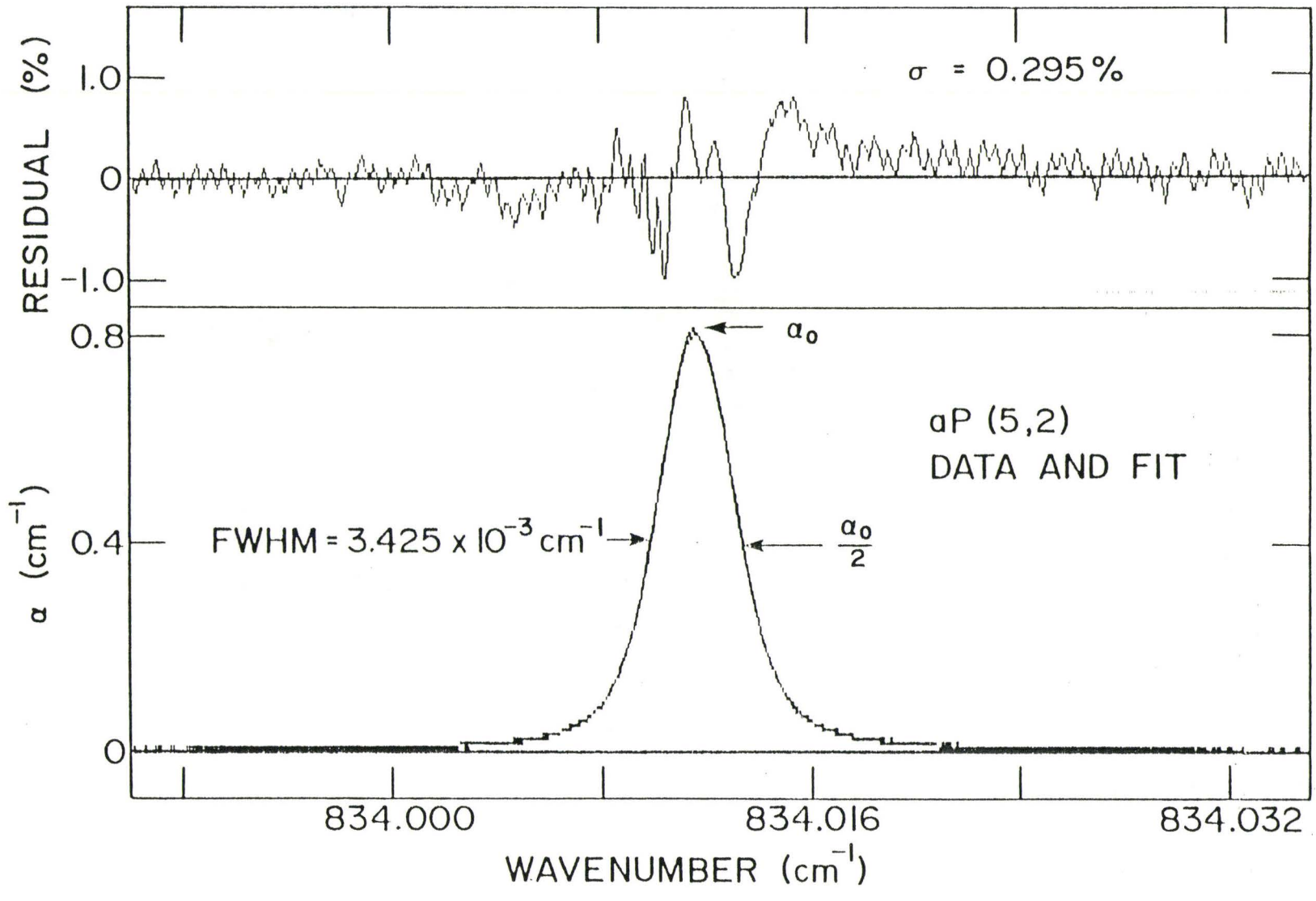
RESIDUAL (%)
1.0
0
-1.0
σ = 0.295 %
0.8
0.4
0
α (cm⁻¹)
α₀
aP (5,2)
DATA AND FIT
FWHM = 3.425 x 10⁻³ cm⁻¹
α₀/2
834.000
834.016
834.032
WAVENUMBER (cm⁻¹)

TABLE 3.1 Line intensities, NH_3-broadened widths, N_2-broadened widths, and Ar-broadened widths in the ν_2 band of NH_3 at 296K. These parameters must be known to determine the NH_3 concentration in the mixture from TDL scans.

Transition	$S_{calculated}$[a] ($cm^{-2}atm^{-1}$)	$S_{measured}$[b] ($cm^{-2}atm^{-1}$)	$\gamma_{NH_3-NH_3}$[c] calculated HWHM (MHz/Torr)	$\gamma_{NH_3-NH_3}$[d] measured HWHM (MHz/Torr)	$\gamma_{NH_3-N_2}$[e] HWHM (MHz/Torr)	$\gamma_{NH_3-N_2}$[d] measured HWHM (MHz/Torr)	γ_{NH_3-Ar}[d] measured HWHM (MHz/Torr)
aR(1,1)	2.68		18.17		4.34(28)		1.91(20)[e]
aP(4,0)	5.14		9.537			3.79(10)	1.63(3)
aP(4,2)	2.06	2.13(5)	17.80	15.59(25)		3.87(8)	1.72(2)
aP(4,3)	2.64		21.93		4.33(27)		
sR(5,0)	6.13		8.915		3.62(20)		
aP(5,1)	1.89		12.46		3.72(8)		
aP(5,2)	1.74	1.78(2)	15.84	14.60(18)			
sP(5,2)	1.83	1.72(8)	15.84	14.72(29)		3.52(12)	1.51(5)
aP(5,3)	2.90		19.22			3.82(18)	1.61(3)
aP(6,0)	2.55		8.915		3.63(9)		
aR(6,0)	3.98		8.877		2.88(10)		
aP(6,1)	1.26	1.30(10)	11.70	11.39(52)	3.50(10)	3.55(2)	1.42(4)
sP(6,1)	1.32		11.70		3.40(31)	3.10(6)	
sP(6,2)	1.27		14.49		3.64(27)	3.47(10)	
sP(6,3)	2.35	2.34(8)	17.27	16.37(30)	3.42(25)	3.71(5)	
sP(7,0)	1.55		8.877			2.69(6)	
sP(7,1)	0.771		11.20		3.15(9)		
sP(7,2)	0.762		13.53		3.35(14)		
sP(7,5)	0.590		20.51			3.41(11)	1.46(3)
sP(7,6)	0.778	0.766(42)	22.84	20.45(77)		3.85(4)	1.75(4)
sP(8,4)	0.398		16.73			3.36(6)	1.27(3)
2sP(4,2)	0.0214[c]	0.0303(23)	17.80	7.85(50)			
2sR(4,3)	0.0611[c]		19.22		3.67(15)		
2sP(5,3)	0.0300[c]	0.0462(8)	19.22	9.02(6)			

(a) Ref. 16

(b) The numbers in brackets represent the estimated accuracy derived from the scatter in linestrength values obtained over an order of magnitude in NH_3 pressure.

(c) Ref. 17

(d) The numbers in brackets represent one standard deviation to the linewidth vs. pressure fits.

(e) Ref. 9

measured by flowing pure NH_3 through a 0.57 cm cell. Linestrengths were calculated from the area under the best fit Voigt profiles. From the accurate measured values of S and γ, the NH_3 content of the gas mixture can readily be calculated. In addition to the immediate need for accurate measurements of foreign gas broadening coefficients, these values are also required for detailed modelling of the NH_3 laser system described in Chapter 2.[1-3]

3.3 The Pump / Probe Setup

Figure 3.2 is a schematic of the experimental apparatus used to determine the vibrational transfer rates in NH_3. A conventional flowing gas cw CO_2 laser tube (120 cm long discharge with a 1.5 cm bore) is placed in a V-shaped cavity formed by a 20 % output coupler mounted on a piezo-electric translator, a spinning mirror and a grating. The PZT and grating are tuned to give stable pulses either on the 9R(30) or 9R(10) CO_2 transitions at 1084.635 cm^{-1} or 1071.883 cm^{-1}. The pulses last < 500 ns, have peak powers of 600 W, and pulse to pulse amplitude stability of better than $\pm$5 %. The pulses are focussed into a 2.5 mm bore pyrex capillary tube which can be varied in length from 5 to 80 cm. The tube allows a high pump intensity ($\simeq$10 kW/cm^2) to be maintained over a long interaction region, and also ensures that the pump and probe beams have good spacial overlap.

The tunable diode laser is combined with the pump

FIGURE 3.2 Schematic diagram of the apparatus used to measure $NH_3(\nu_2)$ lifetimes. The frequency of the TDL can be tuned from 760 to 880 cm^{-1}. The frequency of the Q-switched CO_2 laser can be fine tuned by means of a piezo-electric translator (PZT). Detectors D1 and D2 are Hg-Cd-Te detectors which are used to trigger from the 9 μm pulse, and detect the 12 μm radiation respectively. The dichroic mirror transmits 90% of the 9 μm radiation, and reflects 95% at 12 μm.

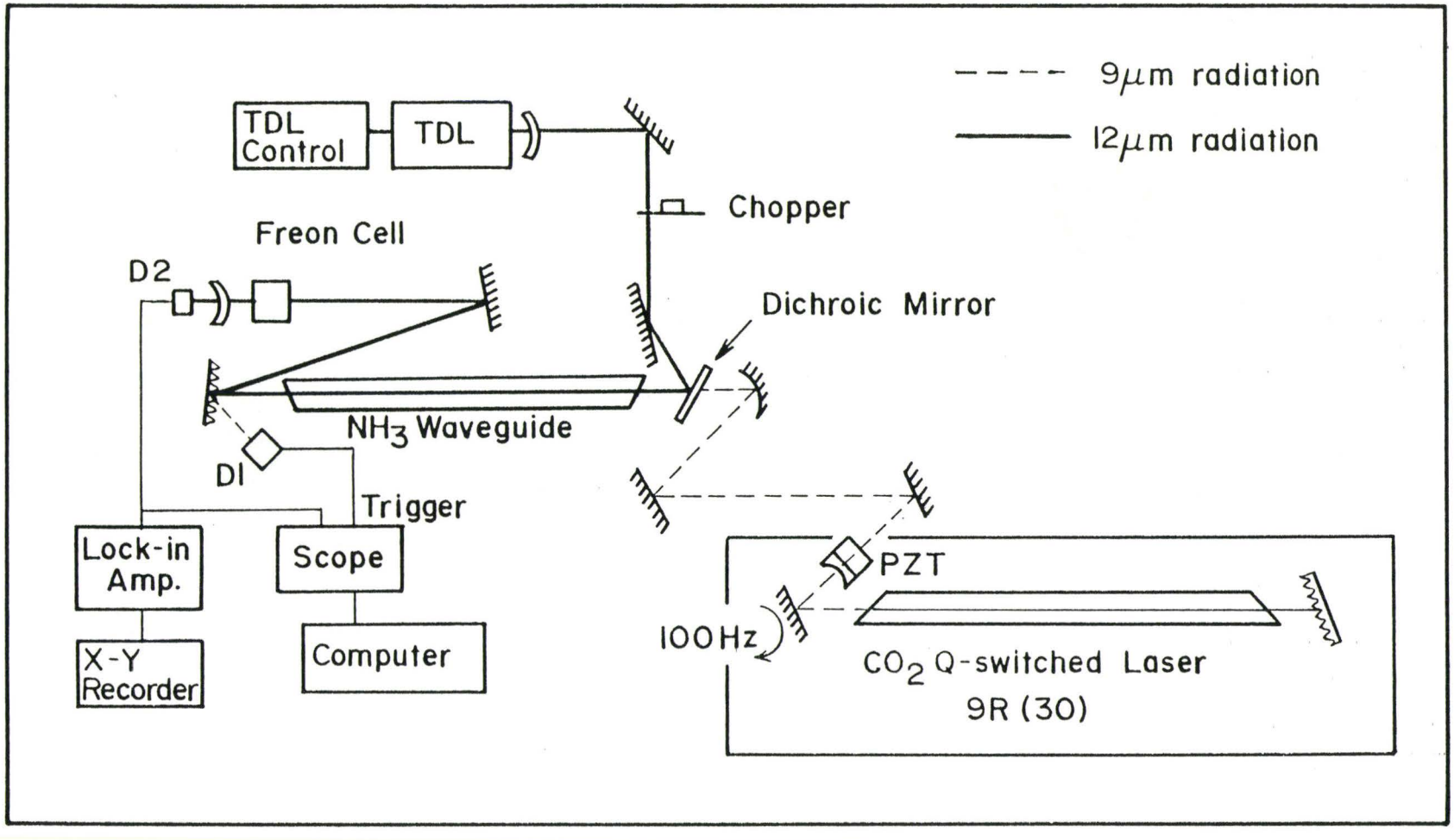
9μm radiation
12μm radiation
TDL Control
TDL
Chopper
Freon Cell
D2
Dichroic Mirror
NH3 Waveguide
DI
Trigger
Lock-in Amp.
Scope
X-Y Recorder
Computer
PZT
100Hz
CO2 Q-switched Laser
9R (30)

beam at a dichroic mirror, and both beams propagate through the empty capillary tube with better than 85 % transmission. The maximum power of the diode laser is 0.2 mW and it can be tuned from 760 to 880 cm^{-1} by changing the temperature of its heatsink and the current in the diode. At the output from the capillary tube the beams are separated by a grating, and a Freon-12 or methanol cell absorbs any remaining CO_2 radiation before the TDL beam is detected by a fast Hg-Cd-Te detector (D2). The effective risetime of the detector and preamp was 250 ns.

Dilute mixtures of NH_3 in N_2 gas were prepared in a 5 ℓ pyrex flask attached to a vacuum manifold. A few Torr of anhydrous NH_3 were added to the empty flask, and the system was allowed to stand until the walls were conditioned. High purity N_2 gas was then passed over liquid N_2 and added to the flask to a total pressure of 600 Torr. The flask was removed from the manifold and attached to one end of the capillary tube, and the gas mixture was slowly flowed through the tube at pressures ranging from 4 to 40 Torr. Total pressure was measured with a capacitance manometer accurate to ±2 %. As a check on the gas composition the TDL output was scanned over several absorption lines in the ν_2 P-branch. The amplitude detection system was the same as used in the S, γ measurements, and typical TDL scans are shown in Figure 3.2. From the measured line center absorption coefficients, and the known linestrengths and pressure

broadening coefficients,[16,18] the NH_3 content of the gas mixture can readily be calculated. TDL measurements of gas composition on several different absorption lines agreed to ±10 %, with a similar agreement between the absorption measurements and the nominal mixture composition as determined by the filling procedure. This method of measuring NH_3 concentration has the advantage that any changes in gas composition within the waveguide can be detected. Adsorption to the cell walls is a problem when using NH_3 gas.

3.4 Measurement of Lifetimes

To measure the lifetime of the ν_2 level, the TDL was tuned to line center of a (ν_2 - ground) transition such as aP(4,0) shown in Figure 3.3. To keep the diode laser locked on line center, a small modulation at 2 kHz was applied to the diode laser current, resulting in a frequency oscillation with peak to peak amplitude < 0.1 linewidth. When the diode laser frequency is scanned and a lock-in amplifier is locked to the modulation frequency a first derivative signal is observed.[19] If this signal is added with the appropriate phase to the small current jitter, the TDL becomes locked to line center of the NH_3 transition. The CO_2 pulsed beam and TDL cw beam were combined at the dichroic mirror and together they propagated through the capillary tube. Since the CO_2 9R(30) transition is only 184 MHz from the NH_3 sR(5,0) transition, population is transferred to the ν_2=1 level in

FIGURE 3.3 CO_2 pump pulse, and the transient decrease in absorption measured by the TDL on the aP(4,0) and aP(4,1) transitions. The inset shows the cw transmission through the capillary tube; the transient measurements were made by locking the TDL successively to points A and B. Measurements were made on a 0.12% mixture of NH_3 in N_2 at a total pressure of 24.8 Torr. The waveguide cell was 81 cm long.

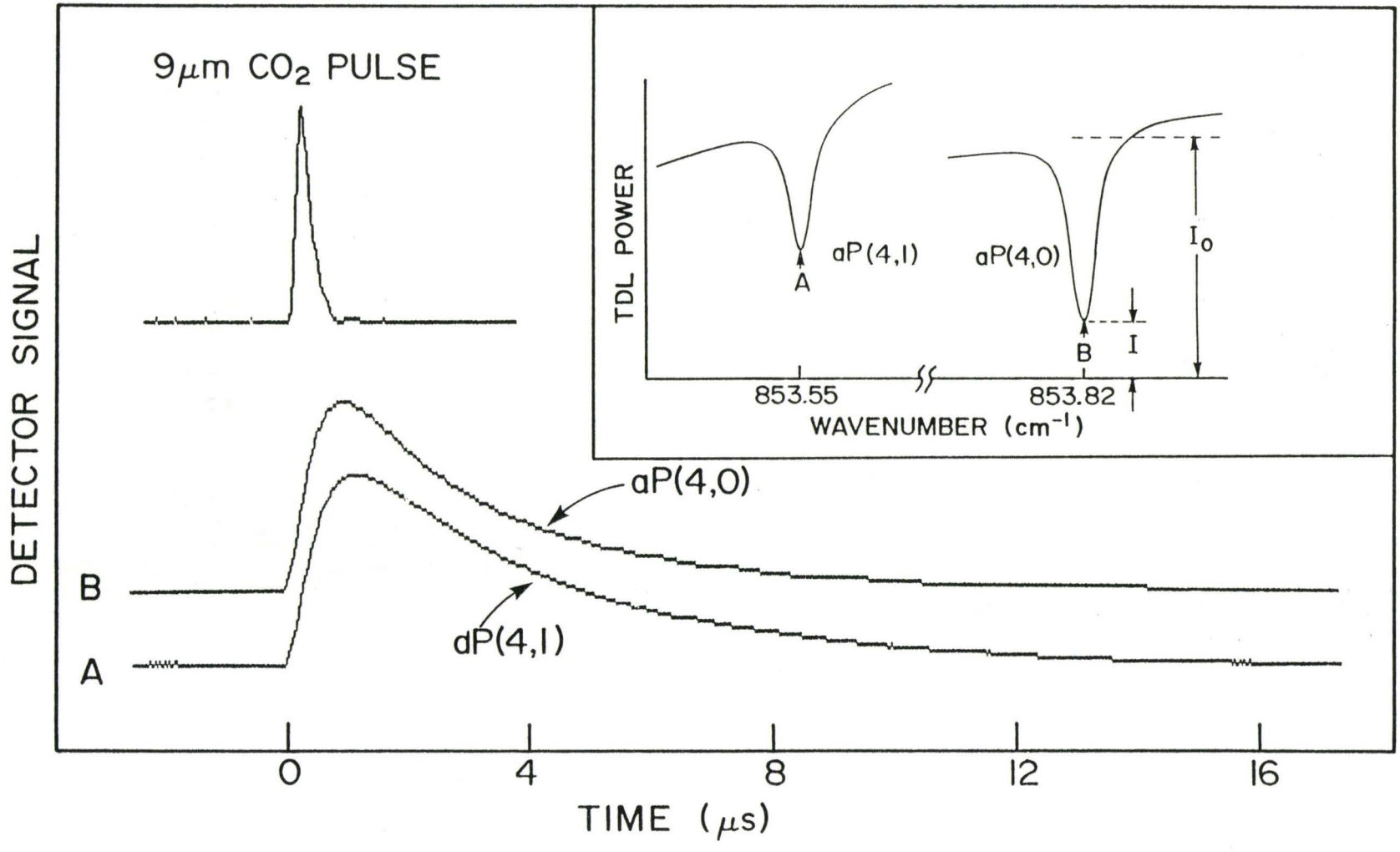
9μm CO2 PULSE
TDL POWER
aP(4,1)
aP(4,0)
A
B
I
Io
853.55
853.82
WAVENUMBER (cm-1)
DETECTOR SIGNAL
aP(4,0)
dP(4,1)
B
A
0
4
8
12
16
TIME (μs)

NH_3 and the absorption on the (ν_2-ground) transitions is decreased.

Transient absorptions were observed on detector D2 in Figure 3.2 and recorded on a Tektronix 468 digital oscilloscope. The 9 μm CO_2 pulse reaching D1 was used to trigger the oscilloscope. The response time of the detection system is limited by the 40 ns per point digitization speed, the ≃250 ns time constant of detector D2 and its preamplifier, and the width of the CO_2 pulse (<500 ns). This detection system is similar to that used by several groups to record transient signals with TDLs.[20,21]

The 9R(30) CO_2 laser transition is 184 MHz from $^{14}NH_3$ sR(5,0) and 340 MHz from $^{14}NH_3$ sR(5,1) and so the ν_2 levels of both ortho (K=3n) and para (K=3n±1) species of NH_3 are populated. Optical pumping directly populates the a(6,0) and a(6,1) ν_2 levels and fast rotational relaxation in the mixture transfers energy to the other vibrational-rotational levels.[1,3] After the CO_2 pumping has ceased, the ortho ν_2=1 rotational levels are in thermal equilibrium with each other, but the ortho and para species may have different vibrational temperatures.[3] The excited populations relax back to the ground state via (V-T) collisional transfer, and the absorption on (ν_2 - ground) transitions also returns to its equilibrium value. For the degree of excitation in the present experiments

$$\frac{\Delta\alpha}{\alpha^e} = C \frac{(N_1 - N_1^e)}{N_1^e} \qquad (3\text{-}1)$$

where α^e is equilibrium line center absorption, $\Delta\alpha$ is the transient change in absorption, N_1^e is the equilibrium value of the population in the v_2 level, N_1 is the transient population in this level, and C is a constant. This relation is based upon the rate equation model discussed in Chapter 2 and described by Morrison.[9] Thus the lifetime of the v_2 level can be obtained from plots of $\Delta\alpha/\alpha^e$ as a function of time. The absorption coefficient is calculated as a function of time from transient signals shown in Figure 3.3 using the relation

$$I = I_0 \exp(-\alpha L) \qquad (3\text{-}2)$$

The cell has length L, and I and I_0 are the incident and transmitted intensity at line center as illustrated in Figure 3.3. The rate equation model indicates that once the CO_2 pump intensity is no longer significant, $\Delta\alpha/\alpha^e$ decays with a time constant, τ, equal to the lifetime of the v_2=1 level.

Figure 3.4 shows a semilog plot of $\Delta\alpha$ vs. time. The PC is used to store the data, calculate $\alpha(t)$, and vary points S and E. The value of τ showed little dependence upon the type of weighting scheme used for the data, so a simple unweighted least squares fit was used. The lifetime τ did not

FIGURE 3.4 Semilog plots of the change in absorption coefficient as a function of time for the aP(4,0) and aP(4,1) transitions. The curvature at the beginning of the plots is caused by residual pumping of the CO_2 pulse, while the steps at the end of the plots are a result of the digital recording technique. The straight lines represent a linear least squares fit to the data between S and E. Measurements were made in a 0.12% NH_3 mixture at 24.8 Torr and 300K.

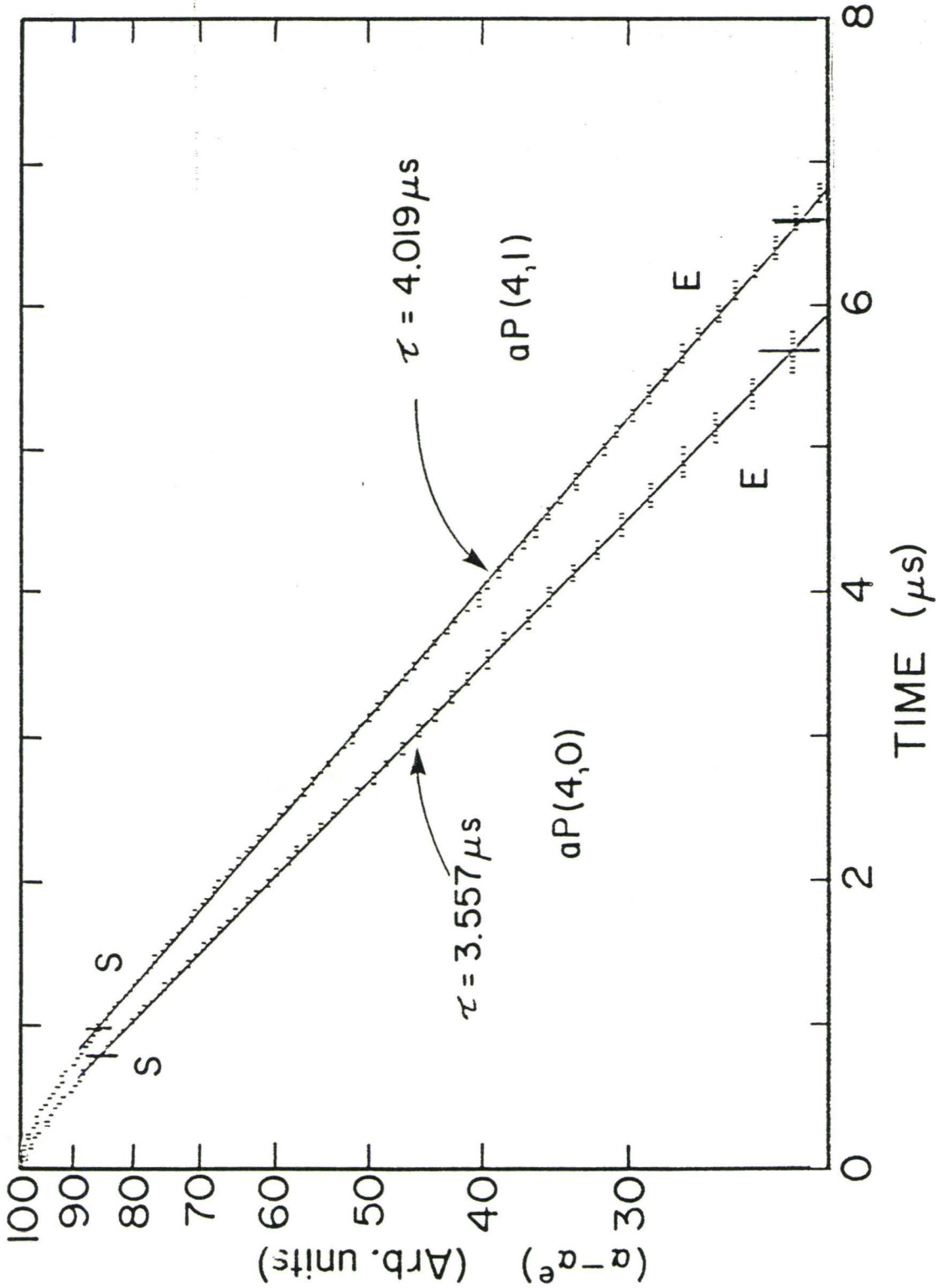
100
90
80
70
60
50
40
30
(a−a^e) (Arb. units)
0
2
4
6
8
TIME (μs)
τ = 4.019μs
aP(4,1)
τ = 3.557μs
aP(4,0)
S
S
E
E

depend on the CO_2 pulse intensity nor upon the exact locking point in the profile of the absorption line. However, as shown in Figure 3.4 there is a significant difference in the decay rate τ depending on which transition is probed by the TDL.[22,23] When several NH_3 transitions were probed the lifetime fell into two groups - those associated with measurements on ortho NH_3 transitions and those associated with para NH_3 transitions. This is shown in Figure 3.5 in which lifetimes for six NH_3 transitions are plotted as a function of pressure. The straight lines are linear least squares fits constrained to pass through the origin. To our initial surprise, the ortho transitions have a shorter lifetime than the para transitions. Radiative transfer of energy is forbidden between ortho and para NH_3. In previous experiments, the ortho and para species of NH_3 were shown to have different degrees of excitation into the ν_2 level.[3] However, 50 % of NH_3 is ortho and 50 % is para, and the ν_2 energy levels are on average the same energy above the ground level for both ortho and para NH_3. Hence the (V-T) relaxation rates are expected to be the same for ortho and para NH_3. Further experiments were necessary to determine the cause of the unexpected difference in lifetime between ortho and para NH_3.

FIGURE 3.5 Plot of the lifetime of the ν_2=1 level, τ, as a function of total pressure for a nominal 2% NH_3 in N_2 mixture. Note the difference in the rate for measurements made on ortho and para transitions. The relaxation process is dominated by NH_3-NH_3 collisions for this mixture.

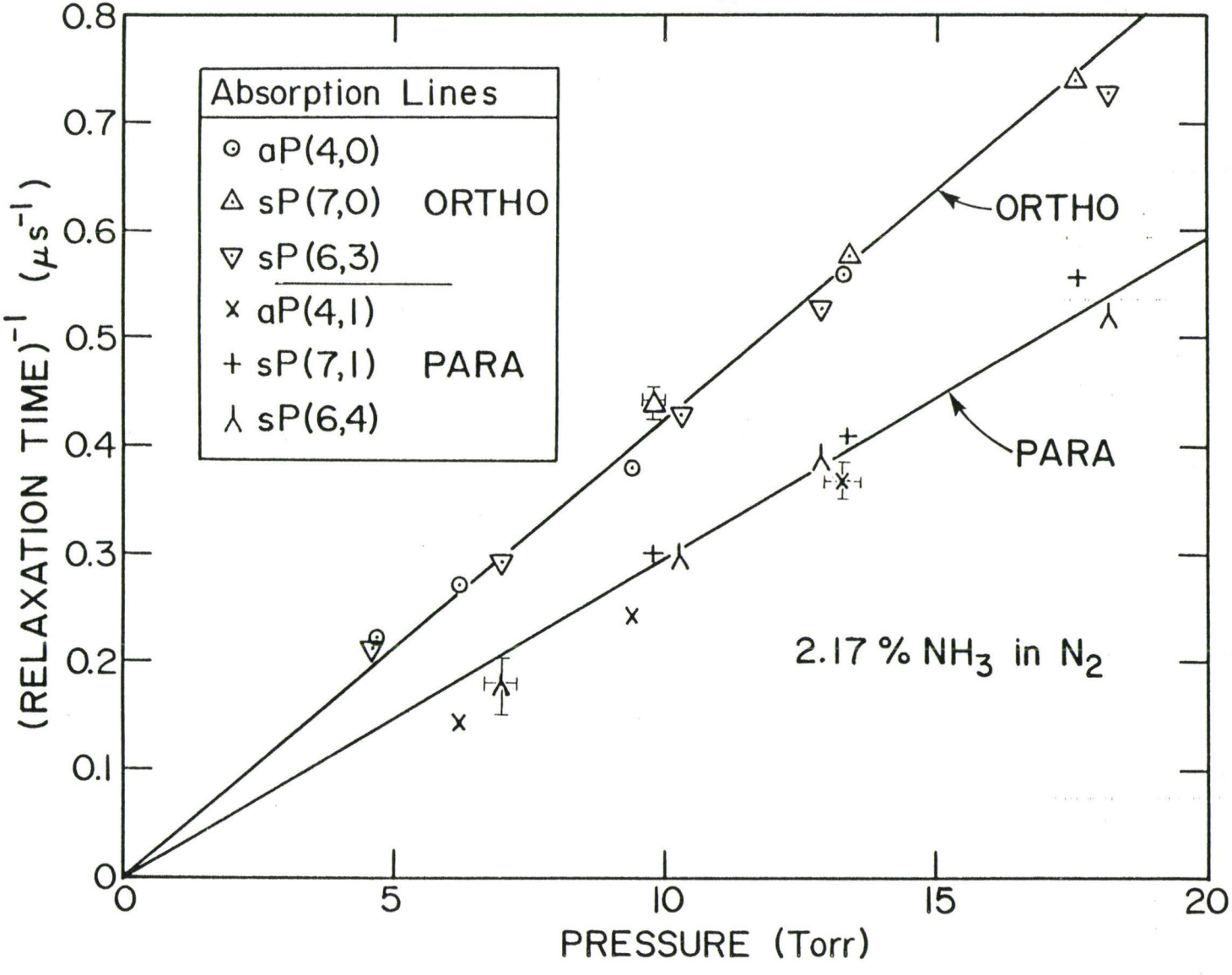
Absorption Lines
aP(4,0)
sP(7,0) ORTHO
sP(6,3)
aP(4,1)
sP(7,1) PARA
sP(6,4)
ORTHO
PARA
2.17 % NH3 in N2
(RELAXATION TIME)-1 (μs-1)
PRESSURE (Torr)
0
0.1
0.2
0.3
0.4
0.5
0.6
0.7
0.8
5
10
15
20

3.5 Conclusion

In previous experiments, the ortho and para species of NH_3 were shown to have different degrees of excitation into the ν_2 level, but it was not expected that these populations would also relax at different rates. Therefore a series of measurements were undertaken to determine if the difference in τ was caused by NH_3 - NH_3 collisions or NH_3 - N_2 collisions, and if the difference could be shown to be the result of (V-V) transfer between ortho and para NH_3. These experiments are discussed in Chapter 4.

Part of the work reported in Chapter 3 is to be published[18] in the Journal of Molecular Spectroscopy. Fig. 3.1 and Table 3.1 were obtained in collaboration with my colleague P. Beckwith.

CHAPTER 4

ANALYSIS AND RESULTS

4.1 Introduction

The purpose of this chapter is to show that NH_3 - NH_3 collisions are responsible for the different measured ν_2 lifetimes for ortho and para NH_3, and that this difference is due entirely to a (V-V) process which also occurs between $^{14}NH_3$ and $^{15}NH_3$. In the first series of experiments, the NH_3 concentration was varied to distinguish between NH_3 - NH_3 and NH_3 - N_2 collisions. Next, a simple rate equation model in which (V-V) transfer of energy between NH_3 species is allowed will be discussed. Finally an isolated ortho $^{15}NH_3$ absorption line is pumped by a CO_2 laser and (V-V) energy transfer to ortho and para $^{15}NH_3$ and $^{14}NH_3$ is observed. The existence of this transfer mechanism was deduced from infrared - microwave double resonance studies by Kano et al.,[7,8] and the tunability of the Pb-salt diode laser is used to probe this energy exchange in detail.

4.2 NH_3 - NH_3 Rates and NH_3 - N_2 Rates

In order to determine whether the difference in the ν_2 lifetime, τ, was due to NH_3 - NH_3 collisions or NH_3 - N_2 collisions, the NH_3 concentration was varied from 0.1 % to 4 %. Figure 4.1 shows results for a 0.1 % mixture. Five

FIGURE 4.1 Repeat of Figure 3.5 for a nominal 0.1% NH_3 in N_2 mixture. In this case the relaxation rate is dominated by NH_3-N_2 collisions.

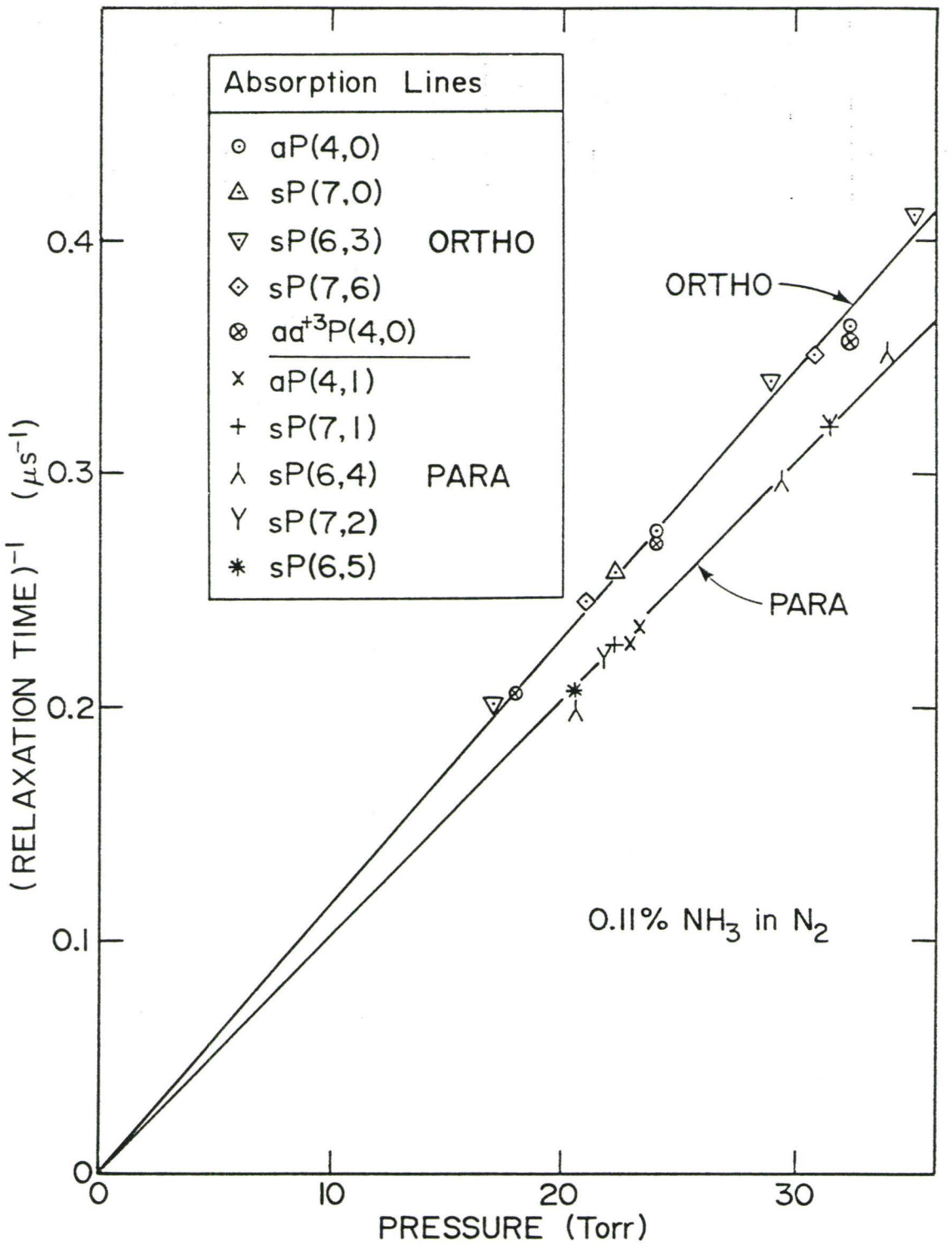
Absorption Lines
aP(4,0)
sP(7,0)
sP(6,3) ORTHO
sP(7,6)
aa+3P(4,0)
aP(4,1)
sP(7,1)
sP(6,4) PARA
sP(7,2)
sP(6,5)
ORTHO
PARA
0.11% NH3 in N2
(RELAXATION TIME)-1 (μs-1)
PRESSURE (Torr)
0
0.1
0.2
0.3
0.4
10
20
30

ortho and five para transitions were investigated, and once again a significant difference in τ was observed. No dependence of this rate on inversion splitting (a -> s or s -> a) was observed. The forbidden transition $aa^{+3}P(4,0)$ transition has antisymmetric[24] upper and lower levels and still gives the same rate as the other ortho transitions. These experiments were limited at low pressures by loss of signal due to lack of absorption of the pump radiation by the narrow absorption lines. The high pressure limit occurs when the relaxation time is on the same time scale as the CO_2 pump pulse. The length of the cell was shortened for high NH_3 concentration mixtures, and lengthened for low concentrations. Figures 4.1 and 3.5 illustrate that the relative difference between ortho and para rates is reduced for lower concentrations of NH_3, and the relaxation rates are identical within experimental error when the NH_3 concentration is extrapolated to near zero. Clearly, NH_3-NH_3 collisions are responsible for the difference between ortho and para relaxation rates.

4.3 (V-T) and (V-V) Transfer

Having established that the difference in τ was due to the NH_3 content in the mixture, the experimental results could be interpreted in two ways: either the existence of a (V-V) transfer mechanism in which vibrational energy is exchanged during collisions between ortho and para NH_3 could

account for the two rates, or the efficiency of the (V-T) process could be faster for ortho than for para NH_3. A simple rate equation model was developed to see if energy transfer between ortho and para NH_3 could account for the results. The model assumes the same (V-T) rate τ_{VT} for each species, and allows for energy transfer between species with a relaxation time, τ_{VV}, where:

$$\frac{1}{\tau_{VT}} = \{(k_{NH_3} - k_{N_2})X_{NH_3} + k_{N_2}\} P \qquad (4\text{-}1)$$

$$\frac{1}{\tau_{VV}} = \{k_{VV} X_{NH_3}\} P \qquad (4\text{-}2)$$

The (V-T) rates associated with NH_3-NH_3 and NH_3-N_2 collisions are k_{NH_3} and k_{N_2}. The rate of energy transfer from one species to the other is k_{VV}. X_{NH3} is the fractional NH_3 concentration, and P is the total gas pressure.

When the CO_2 pump pulse has ended and no further optical pumping takes place, the populations in the ν_2=1 level of NH_3 are assumed to be in rotational equilibrium. However, the ortho and para populations, N_1^O and N_1^P, are not equal and energy transfer takes place from the ortho to the para species at a rate given by $1/\tau_{VV}$. Both the ortho and the para v_2=1 populations are assumed to relax to thermal equilibrium at the same (V-T) time constant, τ_{VT}. With these assumptions, the ν_2 populations can be described by the following equations, once optical pumping has ceased (See

Appendix):

$$N_1^o = c_1 e^{-t/\tau_{VT}} - c_2 e^{-(1/\tau_{VT}+2/\tau_{VV})t} + c_3 \qquad (4\text{-}3)$$

$$N_1^p = c_1 e^{-t/\tau_{VT}} + c_2 e^{-(1/\tau_{VT}+2/\tau_{VV})t} + c_3 \qquad (4\text{-}4)$$

where c_1, c_2 and c_3 are constants which depend only on initial and final conditions, i.e., upon the degree of optical excitation of each species and their thermal values in equilibrium.

The sum and difference of equations (4-3) and (4-4) are:

$$N_1^o + N_1^p = 2c_1 \exp(-t/\tau_{VT}) + 2c_3 \qquad (4\text{-}5)$$

$$N_1^o - N_1^p = 2c_2 \exp\{-(1/\tau_{VT} + 2/\tau_{VV})t\} \qquad (4\text{-}6)$$

Hence, a semilog plot of $(N_1{}^O + N_1{}^P)$ and $(N_1{}^O - N_1{}^P)$ vs. time should be straight lines with slopes $1/\tau_{VT}$ and $(1/\tau_{VT} + 2/\tau_{VV})$, respectively. Figure 4.2 is a semilog plot of $(\Delta\alpha/\alpha^e_{ortho} + \Delta\alpha/\alpha^e_{para})$ and $(\Delta\alpha/\alpha^e_{ortho} - \Delta\alpha/\alpha^e_{para})$ vs. time. Since the absorption coefficients are proportional to $N_1{}^O$ and $N_1{}^P$, the straight line graphs predicted by this V-V model are observed. Similar straight lines were obtained for a series of experiments in which pressures and NH_3 concentrations were varied. Values of τ_{VT} and τ_{VV} were

FIGURE 4.2 Semilog plots of ($\Delta\alpha/\alpha^{e}_{ortho}+\Delta\alpha/\alpha^{e}_{para}$) (upper) and ($\Delta\alpha/\alpha^{e}_{ortho}-\Delta\alpha/\alpha^{e}_{para}$) (lower) vs. time. These straight lines have slopes (τ_{VT}^{-1}) and ($\tau_{VT}^{-1}+2\tau_{VV}^{-1}$) respectively.

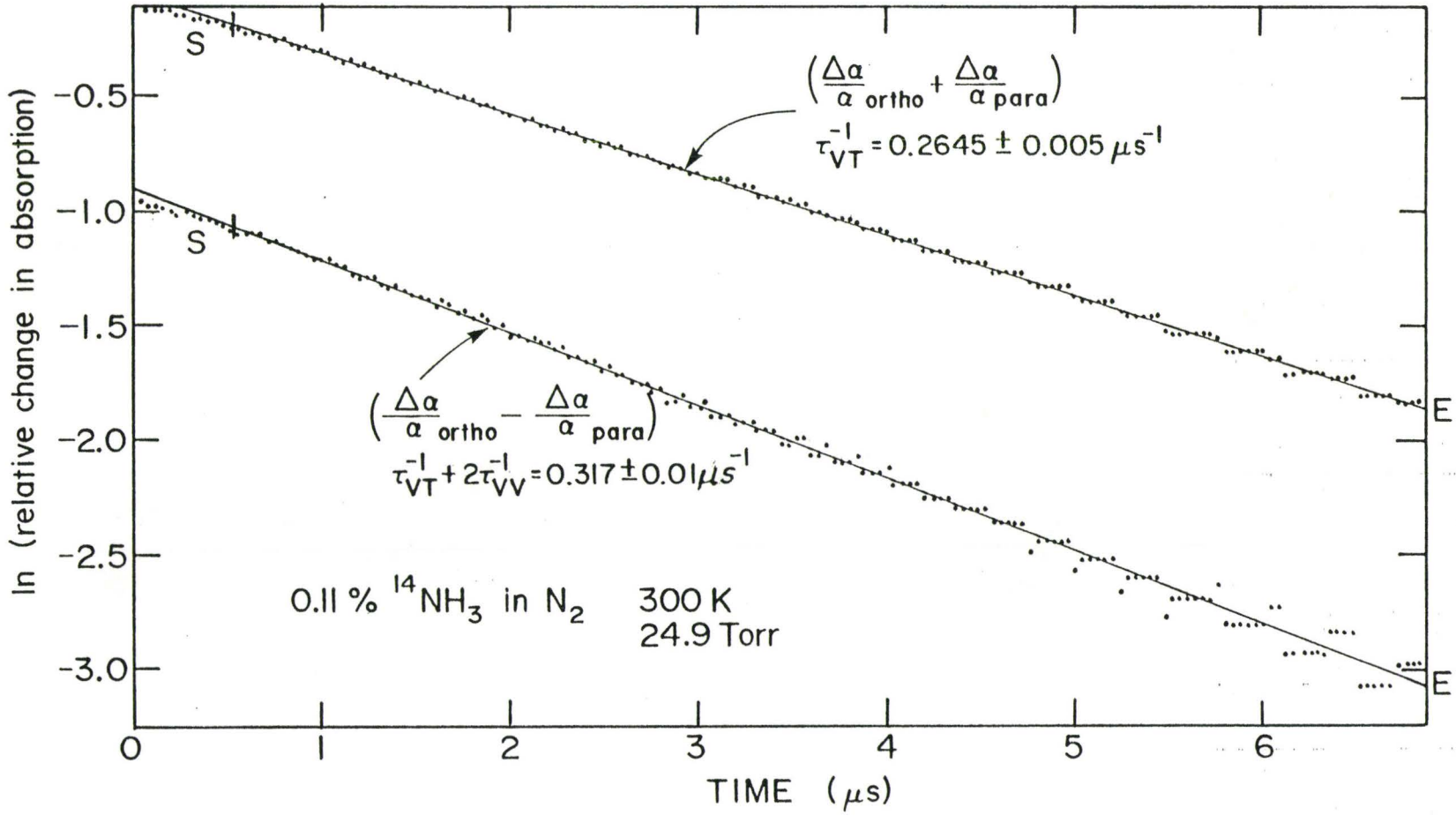
ln (relative change in absorption)
-0.5
-1.0
-1.5
-2.0
-2.5
-3.0
0
1
2
3
4
5
6
TIME (μs)
S
S
E
E
$\left(\frac{\Delta\alpha}{\alpha}_{\text{ortho}} + \frac{\Delta\alpha}{\alpha}_{\text{para}}\right)$
$\tau_{VT}^{-1} = 0.2645 \pm 0.005\ \mu s^{-1}$
$\left(\frac{\Delta\alpha}{\alpha}_{\text{ortho}} - \frac{\Delta\alpha}{\alpha}_{\text{para}}\right)$
$\tau_{VT}^{-1} + 2\tau_{VV}^{-1} = 0.317 \pm 0.01 \mu s^{-1}$
0.11 % $^{14}NH_3$ in N_2 300 K
24.9 Torr

determined as a function of pressure and NH_3 concentration. Several different pairs of ortho and para transitions were probed for a given NH_3 concentration, and Figure 4.3 plots the V-T and V-V relaxation rates as a function of pressure for a 2% NH_3 mixture. Each pair of NH_3 transitions gives the same linear relationship between relaxation rate and pressure. Further confirmation that the model explains the difference in the ν_2 lifetimes is shown in Figure 4.4. In this plot, a variety of mixtures was used, and each mixture was analyzed in the same manner as Figure 4.3. The experimental results are in good agreement with the V-V model, and τ_{VV} depends only upon NH_3 content of the mixture. The V-T rate, τ_{VT}, has some contribution from the buffer gas content, as expected. Hence, all of the measured $^{14}NH_3$ rates are consistent with V-V transfer by the following mechanism:

$$NH_3(1,ortho)+NH_3(0,para)\rightarrow NH_3(0,ortho)+NH_3(1,para) \quad (4\text{-}7)$$

An ideal method of checking that vibrational energy does indeed transfer according to (4-7) is to pump an isolated ortho transition and look for changes in absorption on para transitions. The 9R(30) CO_2 pump was downshifted 180 MHz with an acousto-optic modulator (AOM) such that the pumping radiation is in exact resonance with the sR(5,0) NH_3 absorption line. The 9R(30) pulses were shifted in a manner similar to that described by Kroeker.[13] Unfortunately, since

FIGURE 4.3 Plot of the (V-T) and (V-V) relaxation rates as a function of pressure for a 2% NH_3 in N_2 mixture at 300 K. These rates were determined from semilog plots similar to those shown in Figure 4.2.

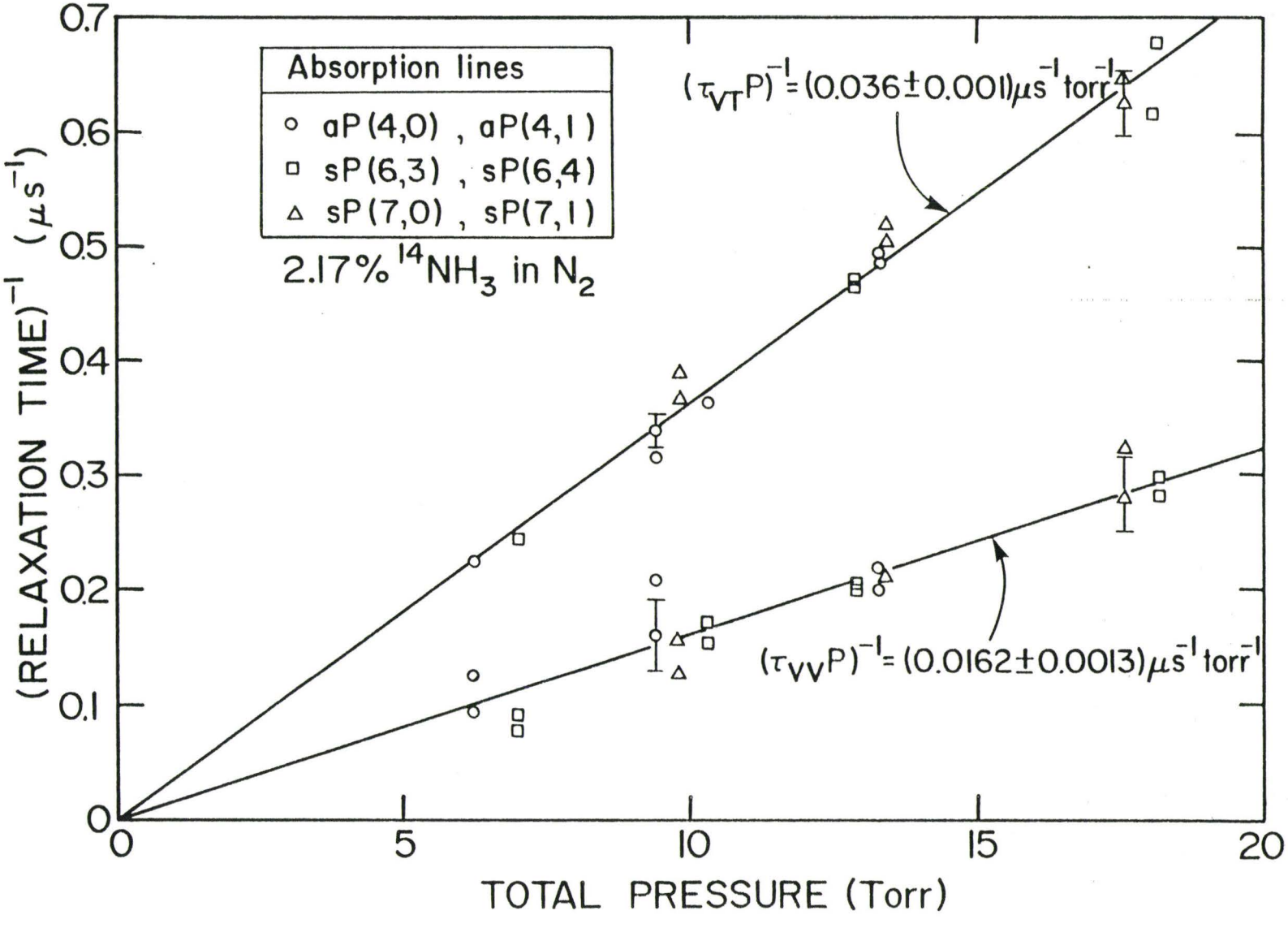
Absorption lines
○ aP(4,0) , aP(4,1)
□ sP(6,3) , sP(6,4)
△ sP(7,0) , sP(7,1)
2.17% $^{14}NH_3$ in N_2
$(\tau_{VT}P)^{-1} = (0.036 \pm 0.001)\mu s^{-1}\,torr^{-1}$
$(\tau_{VV}P)^{-1} = (0.0162 \pm 0.0013)\mu s^{-1}\,torr^{-1}$
(RELAXATION TIME)$^{-1}$ (μs^{-1})
TOTAL PRESSURE (Torr)
0
0.1
0.2
0.3
0.4
0.5
0.6
0.7
5
10
15
20

FIGURE 4.4 Relaxation rates as a function of NH_3 concentration, X_{NH3}. The straight lines are least squares fits to Eq. 4.5 and 4.6. The inset shows an expanded version of the low concentration region.

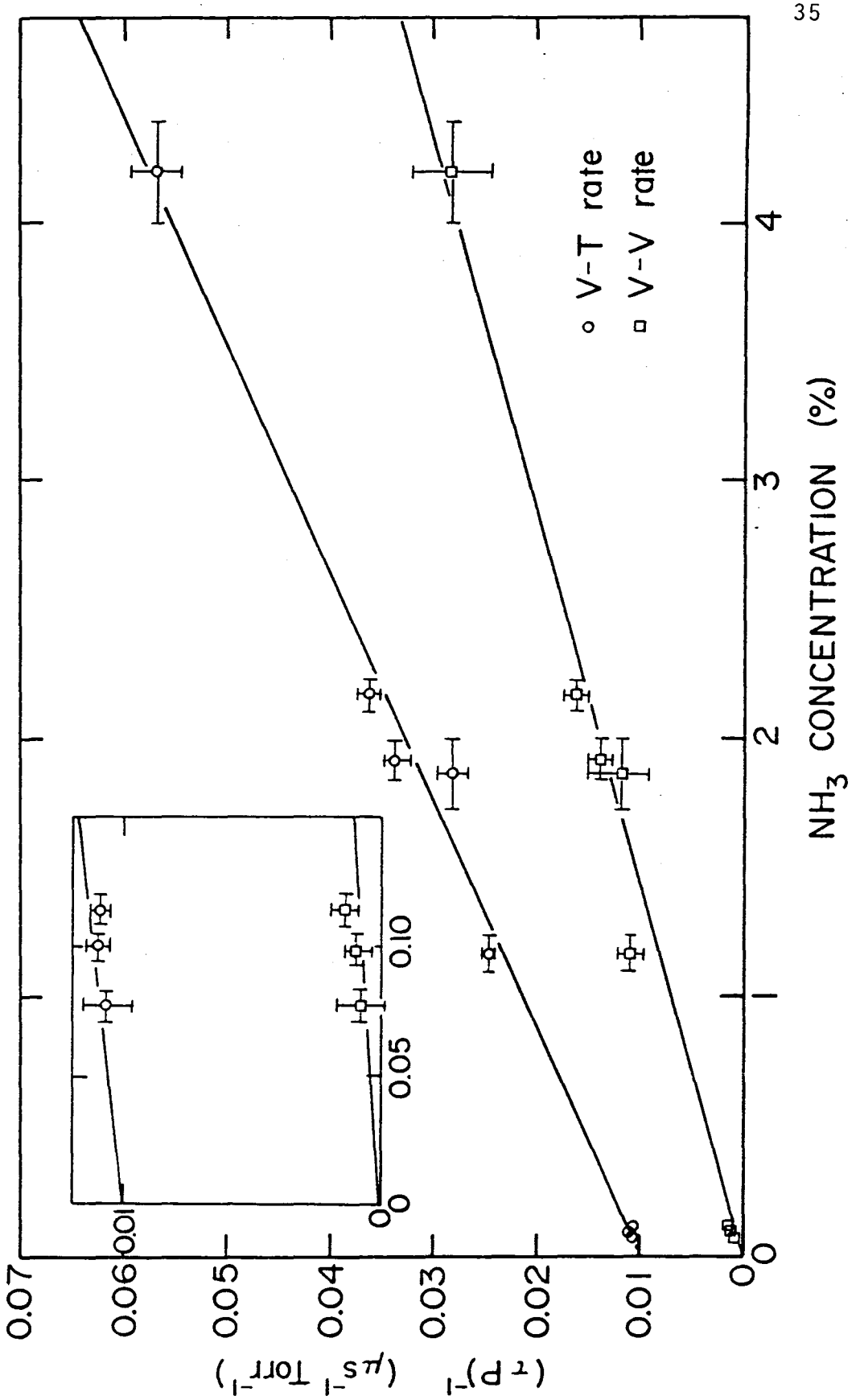
0.07
0.06
0.05
0.04
0.03
0.02
0.01
0
0
1
2
3
4
0.01
0
0.05
0.10
$(\tau P)^{-1}$ (μs^{-1} $Torr^{-1}$)
NH_3 CONCENTRATION (%)
V-T rate
V-V rate

the sR(5,1) NH_3 transition is only 156 MHz away from the sR(5,0) transition, there is still a small amount of direct pumping of the para species. While the experimental results obtained using the downshifted radiation supported the existence of the V-V transfer process, the proximity of the sR(5,1) transition did not allow definitive proof.

Because the absorption lines of NH_3 are spaced widely apart in comparison with individual linewidths, coincidences between CO_2 lasing transitions and NH_3 lines are rare. As a result, convenient $^{12}C^{16}O_2$-$^{14}NH_3$ coincidences which would allow pumping of only one species of NH_3 do not exist. Instead the 9R(10) CO_2 laser line was used to pump $^{15}NH_3$, and the nearest para absorption is > 6 GHz away.[25] As expected, direct optical pumping of the ortho transition resulted in significant population transfer into all the ortho rotational levels in the ν_2=1 level. To enhance sensitivity the $(2\nu_2 - \nu_2)$ transitions were probed by the TDL. Typically, the peak transient absorption was $\sim$7 times the thermal value , as shown in Figure 4.5. A transient increase in absorption was also observed on the $(2\nu_2 - \nu_2)$ para transitions. In this case, the peak value of $\Delta\alpha/\alpha^e$ was approximately unity, but less than 1 % of this change can be accounted for by direct optical pumping or by thermal effects. The magnitude of the direct optical pumping effect was estimated from the known linestrengths and linewidths of the aR(6,0) and aR(6,1) $^{15}NH_3$ transitions and the relative frequency offsets from the

FIGURE 4.5 Observed and calculated $\Delta\alpha/\alpha^{e}_{para}$ as a function of time in a 2% $^{15}NH_3$ in N_2 mixture. In the calculation, (V-T) and (V-V) rates measured from $^{14}NH_3$ observations were used. The calculation assumes no direct optical pumping of para $^{15}NH_3$, and therefore all of the change in ν_2 population is due to the (V-V) transfer process.

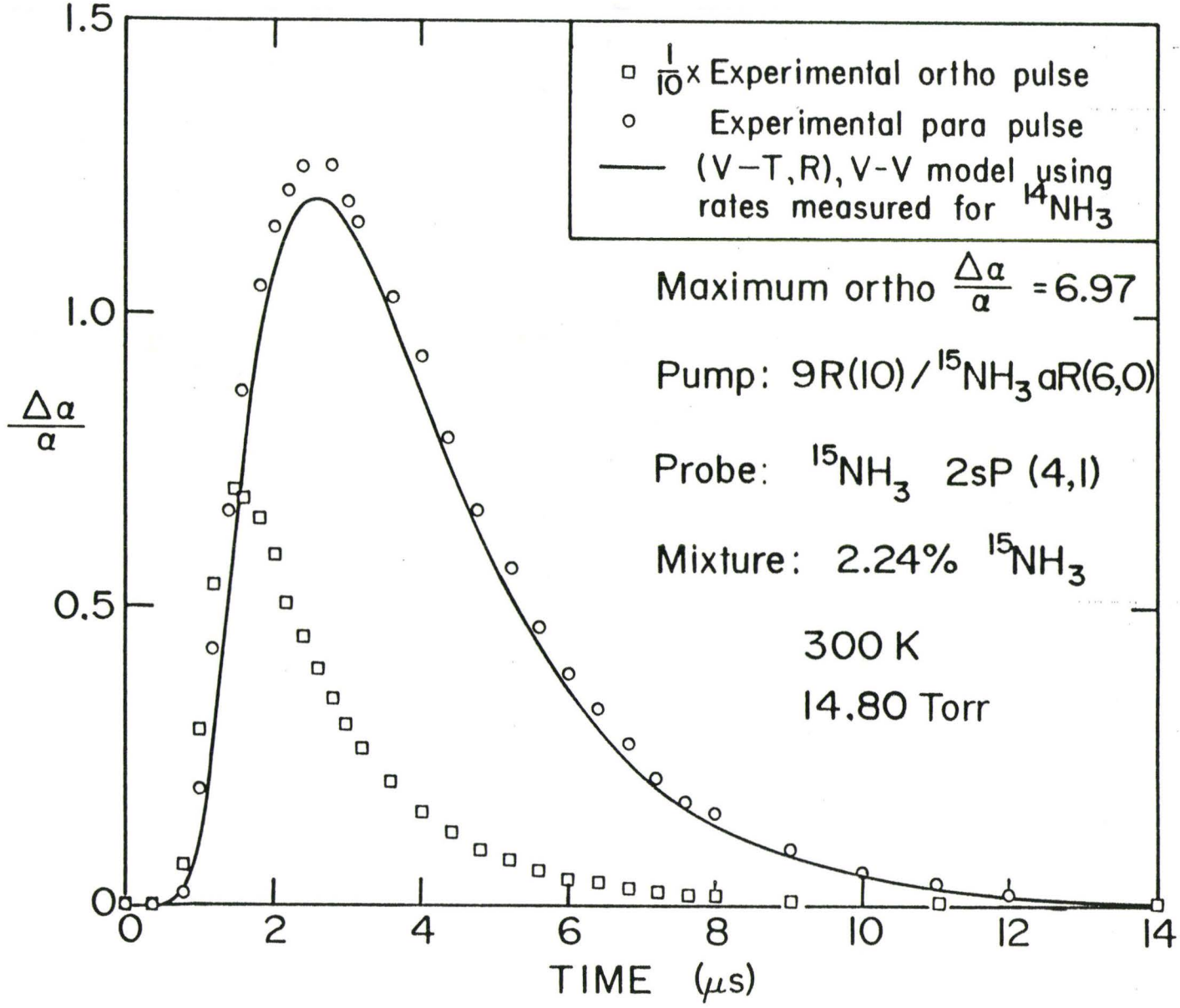
1.5
1.0
0.5
0
$\frac{\Delta\alpha}{\alpha}$
0
2
4
6
8
10
12
14
TIME (μs)
$\frac{1}{10}$ x Experimental ortho pulse
Experimental para pulse
(V−T,R), V-V model using rates measured for $^{14}NH_3$
Maximum ortho $\frac{\Delta\alpha}{\alpha}$ = 6.97
Pump: 9R(10) / $^{15}NH_3$ aR(6,0)
Probe: $^{15}NH_3$ 2sP (4,1)
Mixture: 2.24% $^{15}NH_3$
300 K
14.80 Torr

9R(10) CO_2 laser line. The absorptions were calculated using

$$\alpha = \frac{8\pi^3}{h\lambda_0} |\mu_{ij}|^2 \left(\frac{g_1}{g_2} n_2 - n_1\right) g(\nu) \qquad (4\text{-}8)$$

$$g(\nu) = \frac{1}{\pi\Delta\nu} \frac{1}{1+\{(\nu-\nu_0)/\Delta\nu\}^2} \qquad (4\text{-}9)$$

The width of the lines is $\Delta\nu$ and is known for NH_3/N_2 mixtures. the CO_2 radiation is offset $\nu-\nu_0$ from line center. In formula 4-8, λ_0 is the line center wavelength, h is Plank's constant, μ_{12} is the transition dipole moment, n_2 and n_1 are the upper and lower population densities, g_2 and g_1 are the statistical weights of level 2 and level 1 and $g(\nu)$ is the lineshape. The ratio of $|\mu_{12}|^2$ for the two transitions is equal to the ratio of A_{JK} for the R branch:

$$A_{JK} = [\ (J+1)^2 - K^2\ ] \ /\ [\ (J+1)\ (2J+1)\ ] \qquad (4\text{-}10)$$

The temperature effect was calculated from a pulsed version of the NH_3 laser model developed by Morrison.[9] For the pump powers used in this experiment ($\simeq 5$ kW/cm^2) a change of temperature of $\simeq$1K was predicted. On the 2sP(5,3) transition this corresponds to a change in absorption of 1 % on a timescale much longer than the $\simeq$100 % changes in absorption that were observed on the para $^{15}NH_3$ transitions. The increase in population in the ν_2=1 para levels of $^{15}NH_3$

can only be caused by the (V-V) transfer mechanism given in equation 4.7. This interpretation is confirmed by the calculation of $\Delta\alpha/\alpha^e$ shown in Figure 4.5. The calculation used the measured ortho population and the (V-V) and (V-T) rates from $^{14}NH_3$ as input, and predicted the time-dependent para populations with a high degree of accuracy. Similar results were obtained for other mixtures and pressures in the $^{15}NH_3$ experiments. Clearly the observed difference between the ortho and para relaxation rates is caused by collisional energy transfer from the ortho to the para species.

A similar energy transfer can be expected to occur during collisions between $^{14}NH_3$ and $^{15}NH_3$. A series of experiments were performed using a mixture of 1 % $^{14}NH_3$, 1 % $^{15}NH_3$, and 98 % N_2. Only ortho $^{15}NH_3$ was directly pumped by the 9R(10) CO_2 transition, but transient changes in absorption were observed in ortho and para transitions of both isotopes. Figure 4.6 shows the transient signals observed on ortho and para $^{14}NH_3$ transitions. Also shown are two model predictions ; one using τ_{VV} for a 2 % NH_3 mixture, and one using τ_{VV} for a 1 % mixture. Since (V-V) transfer is taking place between the ortho species of $^{15}NH_3$ and one species of $^{14}NH_3$, one would expect the (V-V) rate to be that of a 1 % NH_3 mixture, while the (V-T) rate should be equal to that of a 2 % mixture. This is confirmed by Figure 4.6. The observed signals are caused by the following ν_2 vibrational energy transfer mechanisms:

FIGURE 4.6 Observed and calculated $\Delta\alpha/\alpha^e$ for ortho and para $^{14}NH_3$ transitions as a function of time in a 1% $^{14}NH_3$, 1% $^{15}NH_3$, 98% N_2 mixture. In the calculation, a (V-T) rate for a 2% $^{14}NH_3$ mixture and a (V-V) rate for a 1% $^{14}NH_3$ mixture were used. A second calculation using a 2% $^{14}NH_3$ (V-V) rate shows that the change in absorption is quite sensitive to the (V-V) rate.

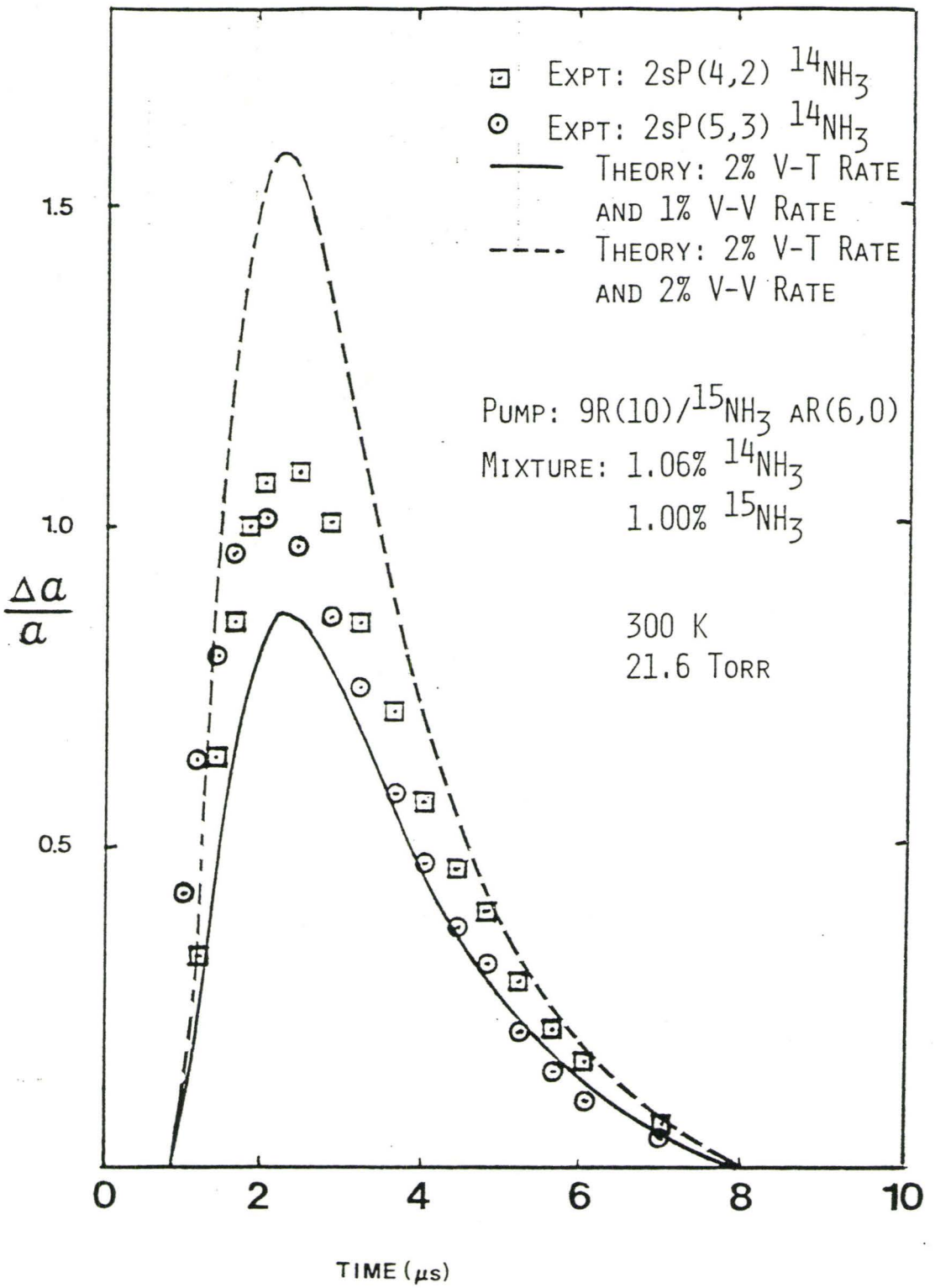
EXPT: 2sP(4,2) $^{14}NH_3$
EXPT: 2sP(5,3) $^{14}NH_3$
THEORY: 2% V-T RATE AND 1% V-V RATE
THEORY: 2% V-T RATE AND 2% V-V RATE
PUMP: 9R(10)/$^{15}NH_3$ aR(6,0)
MIXTURE: 1.06% $^{14}NH_3$
1.00% $^{15}NH_3$
300 K
21.6 TORR
$\frac{\Delta a}{a}$
1.5
1.0
0.5
0
2
4
6
8
10
TIME (μs)

$$^{15}NH_3(1,ortho)+^{15}NH_3(0,para)\rightarrow{}^{15}NH_3(0,ortho)+^{15}NH_3(1,para)$$

$$^{15}NH_3(1,ortho)+^{14}NH_3(0,para)\rightarrow{}^{15}NH_3(0,ortho)+^{14}NH_3(1,para)$$

$$^{15}NH_3(1,ortho)+^{14}NH_3(0,ortho)\rightarrow{}^{15}NH_3(0,ortho)+^{14}NH_3(1,ortho)$$

Within experimental error (± 15 %), the rate constants of these mechanisms appear to be equal, as equal transfer of population was observed from $^{15}NH_3(\nu_2=1$, ortho) to the other three NH_3 species.

Table 4.1 summarizes the results of the measurements of the (V-T) and (V-V) rates. Also included in this table are results obtained at 200 K by packing the capillary tube in dry ice, and a comparison with the results obtained by Hovis and Moore.

4.4 Conclusions

When a Pb-salt diode laser was used to probe transient changes in absorption induced on NH_3 transitions by a pulsed CO_2 laser, a different lifetime for ortho and para transitions was measured. This difference was entirely due to a (V-V) transfer of energy during NH_3-NH_3 collisions. Population changes due only to (V-V) energy transfer were observed on $^{14}NH_3$ and $^{15}NH_3$ transitions. However in inversion NH_3 lasers, the NH_3 concentration is typically 1 % so the

Table 4.1: (V-T)relaxation rates and (V-V) transfer rates between ortho and para NH_3, as measured with a tunable diode laser.

Rate	300K $[\mu s^{-1}\ Torr^{-1}]$	200K $[\mu s^{-1}\ Torr^{-1}]$
k_{NH_3}	1.14 ± 0.05[a]	$1.45 \pm .1$[a]
	1.3 ± 0.2[b]	2.4 ± 0.4[b]
k_{N_2}	$0.0102 \pm .0009$[a]	$0.0075 \pm .0009$[a]
	$.012 \pm .0013$[b]	$.0091 \pm .0014$[b]
k_{vv}	$0.69 \pm .03$[a]	$0.74 \pm .14$[a]

[a]Present measurements

[b]Hovis and Moore,[6] ortho and para populations could not be distinguished.

(V-T) process dominates. Thus, it is only possible to obtain lasing on the particular NH_3 species that is directly pumped.[13,14] In Table 4.1, the results are compared with the values obtained by Hovis and Moore. Although Hovis and Moore only monitored fluorescence from the combined ortho and para levels in NH_3, their results for the (V-T) rates generally agree with our measurements within experimental error. The following chapter investigates the sensitivity of this technique, and includes a summary of related energy transfer phenomena that can be studied.

CHAPTER 5

SENSITIVITY OF THE TRANSIENT DETECTION SYSTEM

5.1 Introduction

In the experiments described in Chapters 3 and 4, the dominant source of noise was digitization noise in the oscilloscope. This is most evident in the semilog plots of $(\Delta\alpha/\alpha^{e}_{ortho}+\Delta\alpha/\alpha^{e}_{para})$ vs. time, where at the end of the pulses the digitization levels are separated. Digitization noise is a result of the relatively small dynamic range of the analog to digital converter in the oscilloscope, and is not related to detector noise. In order to study detector noise on the oscilloscope, a transient signal on the same order of magnitude as this noise must be observed. These experiments are described in Section 5.2. An effort to improve the sensitivity of the detection system with a powerful cw CO_2 laser replacing the TDL is discussed. Finally Section 5.3 outlines future energy transfer studies, and the possibility of a TEA CO_2 pump/ cw NH_3 probe ammonia detector system.

5.2 Sensitivity of Transient Double Resonance Detection

There is much interest in the detection of transient IR absorptions. Radicals which have a short lifetime have been produced by powerful pulsed lasers and detected with cw TDL probes. In another type of transient experiment, the

thermal equilibrium population of a molecular gas is upset with a pulsed laser, as in this study of NH_3. A TDL then monitors the subsequent return to equilibrium and information on energy transfer efficiency can be measured accurately. Both of these experiments are very similar in the sense that a transient absorption change is induced by a powerful pulsed laser and probed by a cw TDL. In the experiments described in Chapters 3 and 4, the sensitivities were limited by digitization noise of the oscilloscope. In contrast, the sensitivity of cw detection systems is limited by optical fringing and beam noise[26] and these levels are much larger than detector noise. Therefore, it is important to eliminate the digitization noise and determine whether the pulsed system sensitivities are limited by beam noise or detector noise.

The digitization noise problem can be easily eliminated simply by observing small transient signals slightly larger than the detector noise. Small transient signals were obtained by lowering the pressure until the NH_3 absorption line sR(5,0) was too narrow to allow efficient pumping by the CO_2 pulses. The signals can also be decreased by lowering the CO_2 power, or by slightly detuning the TDL. The magnitude of the transient signals was decreased until they were on the same order of magnitude as the noise level. Once the transient signals were recorded, the NH_3 gas was removed from the cell and background signals were observed.

Finally the detector noise was recorded (with no CO_2 or TDL beam incident on the detector) so that the noise components could be isolated. Figure 5.1 shows a typical transient signal observed in experiments in Chapters 3 and 4, and a $(2\nu_2-\nu_2)$ transient signal whose size approaches the detector noise level. In the latter case, a change in absorption of 0.06 % was observed with the noise level of 0.01 %. To detect transient signals of this magnitude, a high pass filter was used to cut out noise below $\simeq$10 kHz. The experiment is clearly detector noise limited, and therefore a more sensitive detector or a more powerful cw probe would improve the absorption sensitivity further.

The power of the TDL is optimally $\simeq$ 0.2 mW and so to obtain more power, the probe was switched to a cw CO_2 laser having maximum power output of 3.0 W. However, only 3 mW of probe power could be used before the Hg-Cd-Te detector response became non linear. In order to observe transient signals, the probe laser must be tuned to an NH_3 absorption line. The cw CO_2 laser was tuned to the 9P(24) transition which is in close coincidence to the 2sR(4,3) NH_3 transition.[27] The experimental apparatus is very similar to that described in Chapters 3 and 4, except the CO_2 probe does not have to be frequency locked, and it is off line center from the 2sR(4,3) NH_3 transition. Figure 5.2(I) shows the transient decrease in absorption of the cw CO_2 laser at relatively high NH_3 pressure. When the pressure is lowered,

FIGURE 5.1 Sensitivity of the transient detection system using a TDL. A high pressure signal (.1 % NH_3 in N_2) typical of the signals observed in Chapters 3 and 4 is shown. The lower trace shows the detector noise level and a 0.065% transient pulse (average of 256 pulses) observed with decreased CO_2 power (2% NH_3 mixture at 33 Torr) with the TDL slightly detuned from line center.

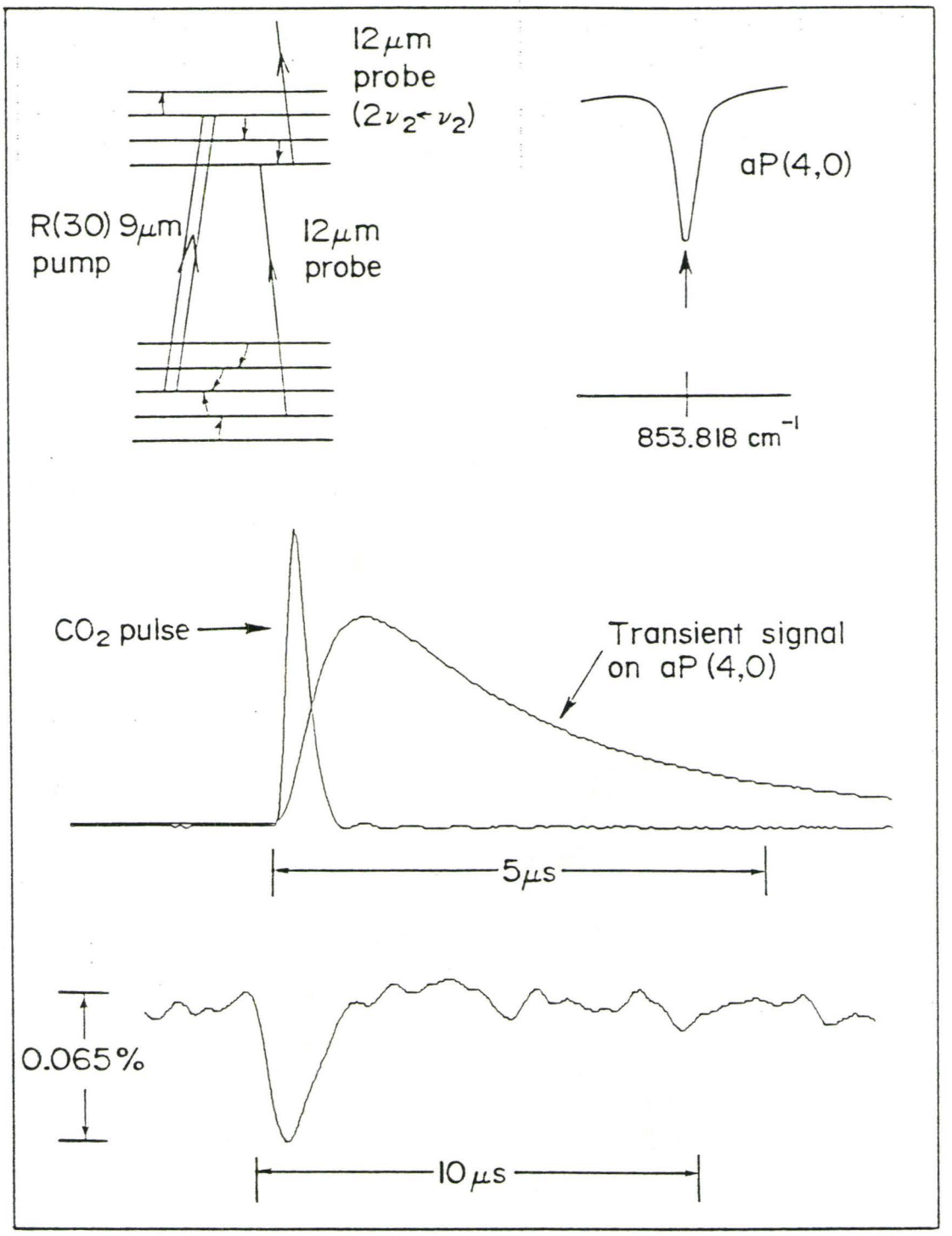
12 μm
probe
(2ν2←ν2)
R(30) 9μm
pump
12μm
probe
aP(4,0)
853.818 cm⁻¹
CO2 pulse
Transient signal
on aP (4,0)
5μs
0.065%
10μs

FIGURE 5.2 Detection of a transient absorption with a cw CO_2 laser as a probe. The upper trace shows a typical high pressure transient signal. Trace A is recorded at lower pressure ($\simeq$1.2 Torr) of a higher concentration NH_3. Background trace B is recorded with no gas in the cell. The background is repeatable so the signal can be subtracted from the background. The resulting sensitivity is detector noise limited and is reduced by averaging 16x256 pulses.

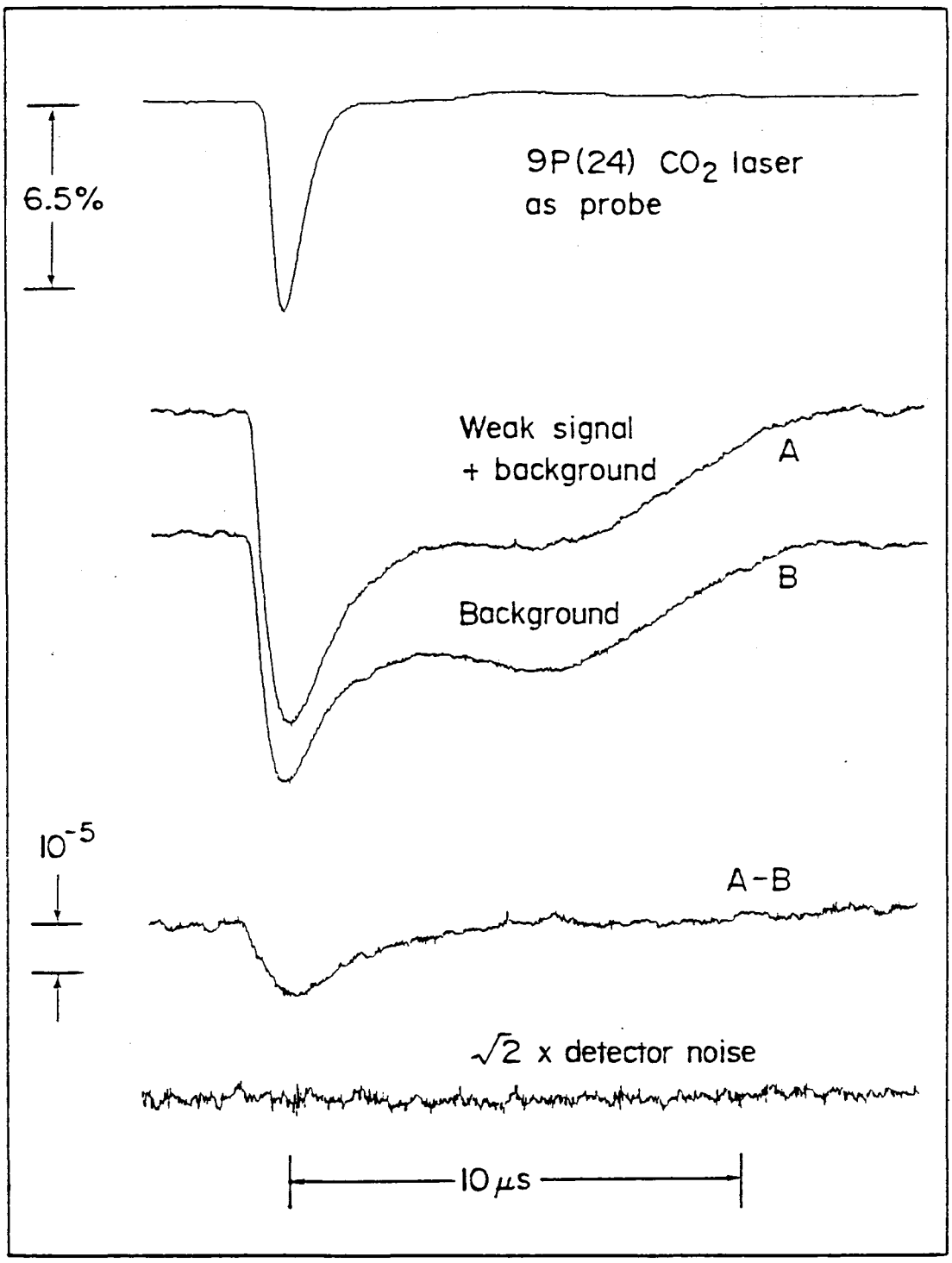
6.5%
9P(24) CO_2 laser
as probe
Weak signal
+ background
A
Background
B
10^{-5}
A-B
$\sqrt{2}$ x detector noise
10 μs

the signals decrease in size and the transient absorptions approach the detector noise level (Figure 5.2(II)). Due to the increased sensitivity of this experiment, a transient decrease in absorption can be observed even though no NH_3 gas is present in the cell. This decrease in absorption is probably due to a small deflection of the probe beam during the CO_2 pulse. With no NH_3 present in the cell, background scans were recorded and subtracted from the NH_3 signal. The result of averaging sixteen X 256 scans are shown in Figure 5.2(III). When the averaged backgrounds are subtracted, a 13 ppm absorption signal was observed with a noise level of $\simeq$ 1 ppm.[28] Hence the sensitivity of the detector noise limited transient detection system can be enhanced by increasing the probe laser power, and by averaging more signals. A similar increase can be expected with a more sensitive detector with a larger dynamic range.

5.3 Future Studies

Since the detection system decribed in this thesis is very sensitive and presently limited by detector noise it may be possible to develop a very sensitive and fast NH_3 detection monitor. Such a monitor would be based upon a powerful TEA CO_2 laser pump combined with a cw NH_3 laser probe copropagating over a long cell length. To develop such an NH_3 monitor, the scalability of the apparatus from a 40 cm waveguide to a very long open path length would have to

be studied to evaluate probe beam deflection problems.

Other energy transfer mechanisms that are suitable for the CO_2 pump/ TDL probe setup include $2\nu_2$ lifetime measurements, and rotational energy transfer rates. The $2\nu_2$ lifetimes are important for accurate modelling of 16 - 21 μm NH_3 lasers[9,29] and the timescale will be approximately the same as the (ν_2 - ground) decay times. The lifetimes could be measured by pumping the 1 % thermal population in the ν_2 level up to the $2\nu_2$ level and probing ($2\nu_2$ - ν_2) transitions, or even ($3\nu_2$ - $2\nu_2$) transitions. The transient signals will be much smaller simply because the available population to pump is much smaller, but the sensitivity of the technique should offset this problem. Another interesting possibility is to pump low pressure NH_3 into a single ν_2 rotational level and observe transfer to other J, K levels. Since only one velocity class is pumped in such an experiment, extremely weak transient signals are expected. The double resonance transient detection system is not limited to NH_3. As long as a pump coincidence can be found, energy transfer mechanisms in many molecular gases can be studied by probing individual vibrational-rotational states with a TDL.

5.4 Conclusion

The CO_2 pump/ TDL probe system is a very sensitive method of detection transient signals, and at present the sensitivity is detector noise limited. As a result, the

sensitivity can be improved by averaging over many pulses, increasing the probe power, or by using a more sensitive detector with a large dynamic range. A cw CO_2 laser near resonance with a $(2\nu_2 - \nu_2)$ NH_3 absorption line was used to improve the sensitivity to near the 1 ppm absorption level. It may be possible to scale the detection system by using a TEA CO_2 / cw NH_3 laser combination to detect NH_3 in the atmosphere. Finally the system is ideal for studying other energy transfer mechanisms in NH_3.

Part of the work reported in this chapter is to be published[28]. Figures 5.1 and 5.2 were obtained with my colleague P. Beckwith.

CHAPTER 6

CONCLUSION

This thesis has presented results of experiments designed to measure collisional transfer of vibrational energy in NH_3. Accurate information on the (V-T) process in NH_3/N_2 mixtures and the (V-V) energy transfer between ortho and para $^{14}NH_3$ and $^{15}NH_3$ is now known. The advantage of using a tunable diode laser to monitor relaxation processes in gases is clearly demonstrated by the measurement of (V-V) transfer in NH_3. A fast, detector noise limited method of monitoring transient absorptions has been developed, with possible applications in the monitoring of atmospheric NH_3.

Many NH_3 linestrengths and linewidths were accurately measured with a TDL so that NH_3 concentrations could be calculated from TDL scans. The vibrational transfer processes were studied by exciting the ν_2 vibration of NH_3 with a Q-switched CO_2 laser and probing the subsequent relaxation of the NH_3 populations with a TDL. When different NH_3 transitions were probed by the TDL, the lifetimes of the ν_2 level fell into two groups - those associated with measurements on ortho NH_3 transitions and those associated with para NH_3 transitions. By varying the NH_3 concentration, the difference in ν_2 lifetimes was shown to result from NH_3 - NH_3 collisions. After remodelling the NH_3 system by including

a (V-V) transfer of energy between the NH_3 species, the difference in lifetimes could be explained by this process. Finally, only the ortho species of $^{15}NH_3$ was excited by the CO_2 laser radiation, and energy transfer to both ortho and para $^{14}NH_3$ and $^{15}NH_3$ was observed, providing evidence of the (V-V) transfer process. The relatively slow (V-V) transfer of energy in dilute NH_3 in N_2 mixtures is consistent with past observations that lasing only occurs on optically pumped species.

The sensitivity of the detection system described in this thesis is presently limited by detector noise. Experiments have shown that the sensitivity can be improved by increasing the probe power, by averaging more pulses, or by using a more sensitive detector. The TDL probe was replaced by a more powerful CO_2 laser, and absorption sensitivities of $\sim$1 ppm were achieved.

In summary, the combination of a pulsed CO_2 laser as an optical pump, and a tunable diode laser as a probe, is a very versatile and sensitive technique for monitoring energy transfer in gases.

APPENDIX

CALCULATION OF τ_{VT} AND τ_{VV} FROM TRANSIENT ABSORPTION SIGNALS

The (V-V) and (V-T) relaxation rates can be related to the changes in absorption of the tunable diode laser. The general form of the rate equation for a gas mixture assuming the molecules are harmonic oscillators is:

$$\frac{dN_n}{dt} = Z \sum [P_{mn}N_m - P_{nm}N_n] + Z/N \sum [Q_{mn}N_iN_m - Q_{nm}N_jN_n] + \left(\sum A_{mn}N_m - \sum A_{nm}N_n \right) \qquad (A\text{-}1)$$

where P_{mn} is the probability per collision of a vibrational-translational exchange, Q_{mn} is the probability per collision of an exchange of quanta from levels m and i to n and j, A_{mn} is the probability of spontaneous radiative transfer from level m to n, N_n is the population of level n, Z is the rate of collisions, and N is the concentration of molecules. Generally, in molecular gases the spontaneous emission rates are orders of magnitude slower than collisional transfer of energy, and so the third bracket can be ignored. For a two level system the time dependence of the upper level can be written

$$\frac{dN_1}{dt} = Z [P_{01}N_0(t) - P_{10}N_1(t)] \qquad (A\text{-}2)$$

but $P_{01} = \exp(-h\nu/kT)\ P_{10} = x_v P_{10}$ so

$$\frac{dN_1}{dt} = -Z\ P_{10}\ [N_1(t) - x_v N_0(t)]. \qquad \text{(A-3)}$$

For a two level system, $N = N_1 + N_0$ so equation A-3 can be rewritten

$$\frac{dN_1}{dt} = -Z\ P_{10}\ (1+x_v)\ [N_1(t) - Nx_v/(1+x_v)]. \qquad \text{(A-4)}$$

The (V-T,R) rate τ_{VT} is defined in terms of energy transfer:

$$\frac{dE_{vib}}{dt} = -1/\tau_{VT}\ [E_{vib} - E^0_{vib}] \qquad \text{(A-5)}$$

where E^0_{vib} is the average vibrational energy at equilibrium, given by

$$E^0_{vib} = \frac{\Sigma e^{-E_n/kT} E_n}{\Sigma\ e^{-E_n/kT}}$$

$$E^0_{vib} = E_1 N x_v/(1+x_v), \qquad \text{and} \qquad E_{vib} = E_1 \Sigma\, n N_n(t)$$
$$= E_1 N_1(t).$$

Then (A-5) becomes

$$\frac{dE_{vib}}{dt} = -1/\tau_{VT}\ [E_1 N_1(t) - E_1 N x_v/(1+x_v)]. \qquad \text{(A-6)}$$

But the rate equation for E_{vib} can also be found using equation A-4:

$$\frac{dE_{vib}}{dt} = \frac{d}{dt} E_1 N_1(t)$$
$$= E_1\ (-ZP_{10})(1 + x_v)[N_1(t) - Nx_v/(1+x_v)]. \qquad \text{(A-7)}$$

Comparing A-6 and A-7, the (V-T,R) rate is

$$(\tau_{VT})^{-1} = ZP_{10}(1+x_v) \qquad \text{(A-8)}$$

$$\therefore \frac{dN_1}{dt} = -1/\tau_{VT}\ [N_1 - Nx_v/(1+x_v)]. \qquad \text{(A-9)}$$

So far only (V-T) transfer has been considered. To include the (V-V) transfer between NH_3 species, consider a

four level system with populations N_0^o, N_0^p, N_1^o, and N_1^p. The (V-V) bracket of equation (A-1) is

$$\frac{dN_1^o}{dt} = (ZQ/N)\,[N_0^o N_1^p - N_1^o N_0^p]. \qquad \text{(A-10)}$$

The population is split equally between ortho and para NH_3:

$$N_1^o + N_0^o = .5N \qquad N_1^p + N_0^p = .5N$$

Eliminating N_0^o and N_0^p one finds

$$\frac{dN_1^o}{dt} = -(1/2\tau_{VV})[N_1^o - N_1^p]. \qquad \text{(A-11)}$$

Hence the rate equations for the upper level of ortho and para NH_3 are

$$\frac{dN_1^o}{dt} = -(N_1^o - C)/\tau_{VT} - (N_1^o - N_1^p)/\tau_{VV} \qquad \text{(A-12a)}$$

$$\frac{dN_1^p}{dt} = -(N_1^p - C)/\tau_{VT} + (N_1^o - N_1^p)/\tau_{VV}. \qquad \text{(A-12b)}$$

[Note: The rates quoted in Ch. 4 are based on equations A-12. To correct for the fact that NH_3 is 50% ortho and 50% para, the (V-V) rates in Table 4.1 should be doubled.]

The above equations can be solved analytically, and the solution is

$$N_1^o = c_1 e^{-t/\tau_{VT}} - c_2 e^{-(1/\tau_{VT}+2/\tau_{VV})t} + c_3 \qquad \text{(A-13a)}$$

$$N_1^p = c_1 e^{-t/\tau_{VT}} + c_2 e^{-(1/\tau_{VT}+2/\tau_{VV})t} + c_3 \qquad \text{(A-13b)}$$

where c_1, c_2, and c_3 are constants which depend upon the relative excitation of ortho and para NH_3, and the thermal population of the upper level. When the solutions are added and subtracted, equations A-13a and A-13b become:

$$N_1^o + N_1^p = 2c_1 \exp(-t/\tau_{VT}) + 2c_3 \qquad \text{(A-14a)}$$

$$N_1^o - N_1^p = 2c_2 \exp[-(1/\tau_{VT}+2/\tau_{VV})t]. \qquad \text{(A-14b)}$$

If the absorption α is calculated as a function of

N_1, the result is:

$$(\alpha - \alpha^e) = C\ (N_1 - N_1^e)$$

where C is a constant. Hence the rates τ_{VT} and τ_{VV} can be obtained directly from the semilog plots of the sum and difference of the ortho and para absorptions.

REFERENCES

1. H. D. Morrison, B. K. Garside, and J. Reid, "Dynamics of the optically pumped mid-infrared NH_3 laser at high pump power," IEEE J. Quantum Electron., QE-20, 1051 (1984).
2. H. D. Morrison, B. K. Garside, and J. Reid, "Gain dynamics in pulsed 12 μm NH_3 lasers," J. Opt. Soc. Am. B., 2, 800, (1985).
3. R. L. Sinclair, J. Reid, H. D. Morrison, B. K. Garside, and C. Rolland, "Dynamics of the line tunable 12 μm cw NH_3 laser as measured with a tunable diode laser," J. Opt. Soc. Am. B., 2, 800 (1985).
4. K. J. Siemsen, J. Reid, and D. J. Danagher, "Improved cw lasers in the 11-13 μm wavelength region produced by optically pumping NH_3," Appl. Opt., 25, 86 (1986).
5. F. E. Hovis and C. B. Moore, "Vibrational relaxation of $NH_3(\nu_2)$," J. Chem. Phys., 69, 4947 (1978).
6. F. E. Hovis and C. B. Moore, "Temperature dependence of vibrational energy transfer in NH_3 and H_2O," J. Chem. Phys., 72, 2397 (1980).
7. S. Kano, T. Amano, T. Shimizu, "Infrared-microwave double resonance studies of collisional-induced transitions and energy-transfer proceeses between vibration-rotation inversion levels in NH_3," J. Chem. Phys., 64, 4711, (1976).

8. N. Morito, S. Kano, Y. Ueda, T. Shimizu, "Double-resonance study of collisional relaxation on frequency coincidence between $\nu_2 R(2,0)$ line of $^{15}NH_3$ and R(42) line of CO_2 laser," J. Chem Phys., 66, 2226 (1977).

9. H. D. Morrison, "Dynamics of optically pumped mid-infrared NH_3 lasers," Ph. D. Thesis, McMaster University, (1984).

10. G. Herzberg, Infrared and Raman Spectra of Polyatomic Molecules (Van Nostrand Reinhold, New York, 1945)

11. C. H. Townes and A. L. Shawlow, Microwave Spectroscopy (Dover, New York, 1975).

12. J. T. Yardley, Introduction to Molecular Energy Transfer (Academic Press, New York, 1980).

13. D. F. Kroeker, "CW mid-infrared NH_3 Lasers," M. Sc. Thesis, McMaster University (1986).

14. D. F. Kroeker and J. Reid, "Line tunable cw ortho- and para- NH_3 lasers operating at wavelengths of 11-14 μm," Appl. Opt., in press.

15. B. H. Armstrong, "Spectrum line profiles - Voigt function," J. Quant. Spectrosc. Radiat. Transfer, 7,61, (1967).

16. R. L. Poynter and J. S. Margolis, "The ν_2 spectrum of NH_3," Mol. Phys., 51, 393 (1984).

17. F. W. Taylor, "Spectral data for the ν_2 bands of ammonia with applications to radiative transfer in the atmosphere of Jupiter," J. Quant. Spectrosc. Radiat. Transfer, 13, 1181 (1973).

18. P. H. Beckwith, D. J. Danagher, and J. Reid, "Linewidths and linestrengths in the ν_2 band of NH_3 as measured with a tunable diode laser," J. Mol. Spectrosc., in press.

19. J. Reid, J. Shewchun, B. K. Garside, and E. A. Ballik, "Point monitoring of ambient concentrations of atmospheric gases using tunable diode lasers," Opt. Eng., 17, 56 (1978).

20. G. A. Laguna and S. L. Baughcum, "Real-time detection of methyl radicals by diode laser absorption at 608 cm^{-1}," Chem. Phys. Lett., 88, 568, (1982).

21. D. Harradine, B. Foy, L. Laux, M. Dubs, and J. I. Steinfeld, "Infrared double-resonance of flouroform-D with a tunable diode laser," J. Chem. Phys., 81, 4267 (1984).

22. D. J. Danagher and J. Reid, "Vibrational relaxation of the ν_2=1 level of ortho and para NH_3," To be published.

23. D. J. Danagher and J. Reid, "Collisional energy transfer in NH_3 measured with a tunable diode laser," TUGG14, IQEC '86, San Francisco, CA.

24. S. Urban, D. Papousek, J. Kauppinen, K. Yamada, and G. Winnewissen, "The ν_2 band of $^{14}NH_3$ - a calibration standard with better than $1x10^{-4}$ cm^{-1} precision," J. Mol. Spectrosc., 101, 1 (1983).

25. G. DiLonardo, L. Fusina, A. Trombetti, and I. M. Mills, "The ν_2, $2\nu_2$, $3\nu_2$, ν_4, and $\nu_2+\nu_4$ bands of $^{15}NH_3$," J. Mol. Spectrosc., 92, 298 (1982).

26. J. Reid, M. El-Sherbiny, B. K. Garside, and E. A. Ballik, "Sensitivity limits of a tunable diode laser spectrometer, with application to the detection of N_2O at the 100 ppt level," Appl. Opt., 19, 3349 (1980).

27. K. J. Siemsen and J. Reid, "Technique for obtaining cw CO_2 sequence lines using an incavity NH_3 cell," Appl. Opt., 17, 3523 (1978).

28. P. H. Beckwith, C. E. Brown, D. J. Danagher, D. R. Smith, and J. Reid, "High sensitivity detection of transient infrared absorptions using tunable diode lasers," To be published.

29. H. D. Morrison, J. Reid, and B. K. Garside, "16 - 21 μm line tunable NH_3 laser produced by 2 step optical pumping," Appl. Phys. Lett., 45, 321 (1984).